Submitted to JGR – Atmospheres (Aura Validation Section), 27 March 2007; revised 30 July 2007

Solar Occultation Satellite Data and Derived Meteorological Products: Sampling Issues and Comparisons with Aura MLS

Gloria L. Manney[1,2], William H. Daffer[3], Joseph M. Zawodny[4], Peter F. Bernath[5,6], Karl W. Hoppel[7], Kaley A. Walker[5,8], Brian W. Knosp[1], Chris Boone[5], Ellis E. Remsberg[4], Michelle L. Santee[1], V. Lynn Harvey[9], Steven Pawson[10], David R. Jackson[11], Lance Deaver[12], C. Thomas McElroy[13], Chris A. McLinden[13], James R. Drummond[8,14], Hugh C. Pumphrey[15], Alyn Lambert[1], Michael J. Schwartz[1], Lucien Froidevaux[1], Sean McLeod[5], Lawrence L. Takacs[10], Max J. Suarez[10], Charles R. Trepte[4], David C. Cuddy[1], Nathaniel J. Livesey[1], Robert S. Harwood[13], and Joe W. Waters[1]

Abstract. Derived Meteorological Products (DMPs, including potential temperature, potential vorticity (PV), equivalent latitude (EqL), horizontal winds and tropopause locations) from several meteorological analyses have been produced for the locations and times of measurements taken by several solar occultation instruments and the Aura Microwave Limb Sounder (MLS). MLS and solar occultation data are analyzed using DMPs to illustrate sampling issues that may affect interpretation and comparison of datasets with diverse sampling patterns, and to provide guidance regarding the kinds of studies that benefit most from analyzing satellite data in relation to meteorological conditions using the DMPs. Using EqL or PV as a vortex-centered coordinate does not alleviate all sampling problems, including those in studies using "vortex-averages" of solar occultation data, and in analyses of localized features (such as polar stratospheric clouds) and other fields that do not correlate well with PV. Using DMPs to view measurements with respect to their air-mass characteristics is particularly valuable in studies of transport of long-lived trace gases, polar processing in the winter lower stratosphere, and distributions and transport of O_3 and other trace gases from the upper troposphere through the lower stratosphere. The comparisons shown here demonstrate good agreement between MLS and solar occultation data for O_3, N_2O, H_2O, HNO_3, and HCl; small biases are attributable to sampling effects or are consistent with detailed validation results presented elsewhere in this issue. The DMPs are valuable for many scientific studies and to facilitate validation of non-coincident measurements.

[1]Jet Propulsion Laboratory, California Institute of Technology, Pasadena, California, USA.
[2]Also at New Mexico Institute of Mining and Technology, Socorro, New Mexico, USA.
[3]Columbus Technologies and Services Inc., Pasadena, California, USA
[4]NASA Langley Research Center, Hampton, Virginia, USA.
[5]University of Waterloo, Waterloo, Ontario, Canada.
[6]University of York, Heslington, York, United Kingdom.
[7]Naval Research Laboratory, Washington, DC, USA.
[8]University of Toronto, Toronto, Ontario, Canada.
[9]LASP, University of Colorado, Boulder, Colorado, USA.
[10]NASA Goddard Space Flight Center, Greenbelt, Maryland, USA.
[11]Met Office, Exeter, United Kingdom.
[12]GATS, Inc., Hampton, Virginia, USA.
[13]Environment Canada, Toronto, Ontario, Canada.
[14]Dalhousie University, Halifax, Nova Scotia, Canada.
[15]University of Edinburgh, Edinburgh, United Kingdom.

1. Introduction

The characterization of atmospheric observations by air mass properties, such as location with respect to the stratospheric polar vortex or the tropopause, is an invaluable tool for research studies and validation. *Butchart and Remsberg* [1986] and *Lait et al.* [1990] mapped atmospheric trace gases with respect to potential vorticity (PV) and equivalent latitude (EqL, the latitude that would enclose the same area between it and the pole as a given PV contour, *Butchart and Remsberg* [1986]). This method is especially valuable in studies using solar occultation satellite data, which comprise no more than 15 profiles per day at each of two latitudes. *Manney et al.* [1999] used PV and EqL to enable detailed study of polar vortex dynamics and transport in ATMOS (Atmospheric Trace Molecule Spectroscopy) data from the ATLAS (Atmospheric Laboratory for Applications and Science) space-shuttle missions; other studies of ATMOS, Halogen Occultation Experiment (HALOE), Polar Ozone and Aerosol Measurement (POAM) II and III, and Stratospheric Aerosol and Gas Experiment (SAGE) II and III data [*Schoeberl et al.*, 1995; *Randall et al.*, 2005, and references therein] have used EqL or PV to help realize the full "condition-space" coverage of the sparse solar occultation datasets. Studies of limb-sounding datasets, such as the Microwave Limb Sounder (MLS) instruments on the Upper Atmosphere Research Satellite (UARS) and Earth Observing System (EOS) Aura missions, and the Michelson Interferometer for Passive Atmospheric Sounding, have also used PV or EqL mapping to study polar vortex dynamics and trace gas evolution [*Manney et al.*, 1995a, 2005a; *Orsolini et al.*, 2005b, and references therein].

Air mass characterization also facilitates comparisons using measurements that are geographically sparse and may not fulfill traditional coincidence criteria based on close matching of time and location. *Santee et al.* [2007a, c, this issue] use EqL as a coordinate to compare Aura MLS data with Upper Atmosphere Research Satellite (UARS) MLS measurements taken in the 1990s. EqL and PV mapping have been used in studies of aircraft and ground-based observations [e.g., *Lait et al.*, 1990; *Redaelli et al.*, 1994]. *Manney et al.* [2001] used EqL mapping, standard geographical coincidence criteria augmented by PV matching, and trajectory histories to compare ozone from seven instruments during the November 1994 period of the ATLAS-3 mission, including four solar occultation instruments (ATMOS, HALOE, SAGE II and POAM II). PV or EqL can be valuable for profile comparisons, providing a means to eliminate comparisons of measurements that may be closely spatially coincident but in different air masses, or to maximize the number of coincidences by allowing comparison of spatially distant measurements taken in the same air mass [e.g., *Michelsen et al.*, 2002; *Lumpe et al.*, 2003; *Chiou et al.*, 2004; *Randall et al.*, 2002].

Several solar occultation datasets are available during the Aura mission, including HALOE, SAGE II and III, POAM III, and the Atmospheric Chemistry Experiment (ACE) Fourier Transform Spectroscopy (ACE-FTS) and Measurements of Aerosol Extinction in the Stratosphere and Troposphere Retrieved by Occultation (MAESTRO) instruments. To facilitate non-coincident validation and intercomparison of measurements sorted by air-mass characteristics, and for use in research studies combining Aura with solar occultation datasets, a set of "derived meteorological products" (DMPs) has been calculated for these solar occultation datasets; the DMPs consist of fields derived from the meteorological analyses interpolated to the locations and times of the satellite observations. DMPs have also been calculated for Aura MLS version 1.5 (v1.5) and version 2.2 (v2.2) datasets; as well as contributing to validation and science studies, these are used in producing plots for routine inspection of MLS data, and daily EqL/potential temperature (θ) cross-sections that are posted on the MLS website [http://mls.jpl.nasa.gov]. In the following, we document the DMPs for the solar occultation instruments and MLS and use them for comparisons of solar occultation and MLS data. We explore effects of the satellites' diverse sampling patterns, to provide guidance as to types of comparisons and scientific studies in which DMPs are most valuable. DMPs for MLS and/or solar occultation instruments are used in MLS validation in other papers in this issue [e.g., *Santee et al.*, 2007a, c]; DMPs have been used in several recent studies of solar occultation data, including validation comparisons [e.g., *Chiou et al.*, 2004; *Thomason et al.*, 2006] and scientific analyses [e.g., *Dufour et al.*, 2005; *Nassar et al.*, 2005; *Rinsland et al.*, 2005; *Jin et al.*, 2006b].

2. Dataset Descriptions

2.1. Solar Occultation Datasets

2.1.1. ACE-FTS SCISAT-1, also known as ACE, was launched August 2003 [*Bernath et al.*, 2005]. The primary instrument is the ACE-FTS, a Fourier transform spectrometer featuring high resolution (0.02 cm^{-1}, corresponding to a $\pm$25 cm maximum optical path difference) and broad spectral coverage in the infrared (750-4400 cm^{-1}). ACE-FTS works primarily in the solar occultation mode, collecting atmospheric limb measurements using the sun as a radiation source. Version 2.2 of the ACE-FTS retrievals [*Boone et al.*, 2005] is used here, except for O_3, for which the ACE-FTS product known as "version 2.2 ozone update" is used. Early validation efforts with the ACE-FTS data identified a roughly 10% low bias for altitudes near the O_3 concentra-

tion peak when compared to other satellite measurements, and a ∼25–30% high bias near 45–50 km [*Walker et al.*, 2005; *Fussen et al.*, 2005; *Petelina et al.*, 2005]. Version 2.2 processing uses microwindows in two spectroscopic regions: 1000-1150 cm^{-1} and 1800-2150 cm^{-1}. Version 2.2 O_3 update uses microwindows in the 950-1150 cm^{-1} range and, in preliminary comparisons, exhibits improved agreement with other datasets near the O_3 concentration peak; a comprehensive validation exercise for the ACE-FTS v2.2 O_3 update is being completed [*E. Dupuy, et al., "Validation of ozone measurements from the Atmospheric Chemistry Experiment (ACE)", in preparation*]. ACE-FTS vertical resolution is ∼3–4 km. Latitudes of measurements vary over an annual cycle with coverage as high as ±85° and an emphasis on the polar regions in winter and spring. Separate files with ACE-FTS geolocation information, primarily latitude and longitude as a function of altitude, are provided for each occultation; for occultations with missing geolocation files, the geolocation information is taken from the headers of the data files, which give 30-km tangent point latitude and longitude values; most differences are small, but can be up to ∼3° latitude and ∼10° longitude for brief periods, depending on the viewing geometry. The data downlink capacity available for ACE early in the mission was ∼2 Gb/day [*Bernath et al.*, 2005], limiting the number of occultations that could be recorded; the downlink was increased in March 2005, and now almost all available occultations are measured during most of the year.

2.1.2. MAESTRO The MAESTRO instrument is the secondary instrument on the SCISAT-1 (ACE) payload. It comprises two miniature, photo-diode array spectrophotometers designed to cover the wavelength range 285 to 1015 nm. O_3 slant column amounts are determined by spectral fitting of the data between 530 and 755 nm in the version 1.2 (v1.2) dataset used here. Slant column amounts are inverted to produce vertical profiles of O_3 mixing ratio [*McElroy et al.*, 2007]. MAESTRO slant column amounts are retrieved using pressure-temperature profile data and tangent height-time information from ACE-FTS. The vertical resolution of MAESTRO O_3 is ∼1.2 km [*Kar et al.*, 2007]. MAESTRO sunset profiles are very consistent with the ACE-FTS profiles except for a few percent from measurements taken between 20:00 and 24:00 UT. An analysis of the apparent altitude shift between these MAESTRO and FTS profiles indicates that there is a 1-second time shift during this period. The sunrise profiles have a time error increasing from zero to one second between 00:00 and 24:00 UT. Since MAESTRO uses the FTS-derived tangent height tables, a time shift between FTS and MAESTRO will introduce an artificial shift in the MAESTRO tangent heights of a few km; this results in mixing-ratios that can be significantly low or significantly high, depending on the size of the time shift. While a method to objectively identify and correct these shifts based on MAESTRO internal information is under development, the v1.2 profiles have not be corrected for this artifact. MAESTRO sunrise and sunset O_3 profiles show opposite biases with respect to SAGE III and POAM III, with sunset values in the upper stratosphere being up to ∼30% higher than those instruments, and sunrise values up to ∼15% lower in most of the stratosphere [*Kar et al.*, 2007].

2.1.3. HALOE HALOE [*Russell et al.*, 1993] was operational on the Upper Atmosphere Research Satellite (UARS) from October 1991 through November 2005. HALOE observations take approximately one month to cover the full range of latitudes sampled (ranging from ±80° to ±50°, depending on season, reaching highest (lowest) latitudes in summer (winter)). Estimates of uncertainties for the profiles of the retrieved HALOE parameters from its first public release dataset (Version 17) are provided in *Journal of Geophysical Research, Atmospheres, 101, D6* – a special UARS Validation Issue published in 1996. The data used here are Version 19. Some updated uncertainty estimates for Version 19 are available for O_3 [*Randall et al.*, 2003], H_2O [*Kley et al.*, 2000], and temperature *Remsberg et al.* [2002]. Vertical resolution is ∼2 km for O_3 and H_2O, ∼3–4 km for temperature, and ∼4 km for HCl. Temperatures in the HALOE files below 35 km are from the NCEP/CPC meteorological analyses. HALOE latitude and longitude as a function of height are provided on the same 0.3-km grid used for the temperature files.

2.1.4. POAM POAM II [*Glaccum et al.*, 1996] and POAM III [*Lucke et al.*, 1999] were visible/near-infrared solar occultation instruments that typically made 14-15 measurements per day in each hemisphere around a circle of latitude with a longitudinal spacing of about 25°. The latitudinal coverage was identical each year, slowly varying between 54°N - 71°N and 65°S - 88°S. POAM II obtained data from October 1993 until November 1996, when the host satellite failed; POAM III obtained data from late April 1998 through early December 2005. POAM II provided measurements of O_3, aerosol extinction, and NO_2; POAM III provided H_2O in addition to these. The POAM III Version 4 ozone retrievals differ little from the Version 3 retrievals described by *Lumpe et al.* [2002], and validated by *Lumpe et al.* [2003] and *Randall et al.* [2003]. At 15 km and above, the O_3 retrievals have a vertical resolution of ∼1 km and an estimated precision of 5% [*Lumpe et al.*, 2002]. The H_2O retrievals extend from 5 to 50 km with 5-7% precision and a vertical resolution ranging from 1 km in the lower stratosphere to 3 km in the upper stratosphere. The H_2O retrievals have been validated by *Lumpe et al.* [2006]. Geolocation information (latitude,

longitude and line-of-sight (LOS) angle) for POAM III were calculated on an 8-km grid, and interpolated linearly to the POAM 1-km measurement grid.

2.1.5. SAGE II SAGE II [http://science.hq.nasa.gov/-missions/satellite_45.htm] used radiances at 600 nm to derive O_3 and at 940 nm to derive H_2O; it took measurements from October 1984 through August 2005. The instrument and earlier versions of the retrieval algorithm, as well as O_3 validation, are discussed by *Chu et al.* [1989], *Cunnold et al.* [1989], and *McCormick et al.* [1989]. SAGE II data used here are Version 6.2. O_3 data have ∼1 km or better vertical resolution, and H_2O data no better than ∼1 km. Validation of v6.1 O_3 is discussed by *Wang et al.* [2002]; *Wang et al.* [2006b] show some correlative data comparisons with v6.2 O_3. H_2O validation is discussed by *Chiou et al.* [2004] and *Taha et al.* [2004]. The precision of SAGE II O_3 is estimated to be ∼2% [*Borchi and Pommereau*, 2006] and no credible estimates of the precision of H_2O measurements exist. The SAGE II coverage follows a pattern similar to that of HALOE. Geolocation information, including line-of-sight (LOS) angle, was provided on the measurement grid in separate files.

2.1.6. SAGE III The SAGE III instrument [http://science.hq.nasa.gov/missions/satellite_8.htm] used radiances from several channels in the 570 to 600 nm region to derive O_3 and at several more in the 925 to 960 nm region to derive H_2O (though H_2O retrievals are not yet available); it took measurements from May 2002 through December 2005. The instrument and the retrieval algorithm, as well as O_3 validation, are discussed by *Mauldin et al.* [1985], *McCormick et al.* [2002], and *Wang et al.* [2006a]. SAGE III data used here are Version 3 "MLR" O_3, which has a vertical resolution of ∼1 km. The precision of SAGE III O_3 has not been objectively estimated but should be comparable to SAGE II. SAGE III solar measurement coverage from the sun synchronous orbit is confined to mid to high latitudes with sunrise events in the southern hemisphere (∼30–50°S) and sunset events in the north (∼50–80°N). Geolocation information is included in the SAGE III data files every 10 km in the vertical; this is interpolated linearly to the 0.5-km data grid.

2.2. Aura MLS Dataset

MLS measures millimeter- and submillimeter-wavelength thermal emission from the limb of Earth's atmosphere. Detailed information on the measurement technique and the MLS instrument on the EOS Aura satellite is given by *Waters et al.* [2006]. The Aura MLS fields-of-view point in the direction of orbital motion and vertically scan the limb in the orbit plane, leading to data coverage from 82°S to 82°N latitude on every orbit. Vertical profiles are measured every 165 km along the suborbital track and have a horizontal resolution of ∼200–300 km along-track and ∼3–9 km across-track. Vertical resolution of the Aura MLS data is typically ∼3–4 km in the stratosphere, depending on the product. *Livesey et al.* [2007b], as well as papers on individual MLS products (listed below), provide detailed precision and resolution information for for v2.2 MLS data.

Examples using DMPs to compare many of the species retrieved from MLS measurements with solar occultation data are presented here. Comprehensive validation of these species for v2.2, including detailed precision and resolution information, is done in papers in this issue: *Lambert et al.* [2007] (N_2O and H_2O), *Froidevaux et al.* [2007b], *Jiang et al.* [2007], *Livesey et al.* [2007a], and references therein (O_3), *Froidevaux et al.* [2007a] (HCl), *Santee et al.* [2007c] (HNO_3), *Pumphrey et al.* [2007] and *Livesey et al.* [2007a] (CO), and *Schwartz et al.* [2007] (temperature). Initial validation comparisons of v1.5 MLS data are given by *Froidevaux et al.* [2006] and *Barrett et al.* [2006]. Reprocessing with MLS v2.2 is ongoing at the time of writing, and will be complete by mid-2008; the comparisons shown here use v2.2 data, except one example that uses v1.5 data to illustrate sampling effects over a full season (section 3.2).

2.3. Meteorological Analyses

DMPs are currently calculated from the Met Office (MetO) dataset for each of the instruments, from the NASA Global Modeling and Assimilation Office's (GMAO) Goddard Earth Observing System (GEOS) datasets (4 and/or 5) for MLS and ACE-FTS, and from the NCEP/CPC (National Centers for Environmental Prediction/Climate Prediction Center) analyses for SAGE II. A brief description of these datasets follows; further information is given by *Manney et al.* [2005b, and references therein], which also provide comparisons between these and other meteorological datasets.

The MetO data through 12 March 2006 are from the stratosphere-troposphere (STT) data assimilation system first developed for the Upper Atmosphere Research Satellite (UARS) project [*Swinbank and O'Neill*, 1994], and have been produced since October 1991. The assimilation used an analysis-correction scheme as described by *Lorenc et al.* [1991] until late 2000, when a three-dimensional variational (3D-Var) scheme was implemented [*Lorenc et al.*, 2000]. In late 2003, a new dynamical core [*Davies et al.*, 2005] was implemented in the assimilation system [*Swinbank et al.*, 2002, 2004]. The MetO-STT data (three-dimensional winds, temperature, and geopotential height) are supplied once-daily at 12UT on a 2.5° latitude by 3.75° longitude grid, and at UARS pressure levels (6 levels per decade in pressure) between 1000 and 0.3 hPa (0.1 hPa after late 2003).

After 12 March 2006, the stratospheric analyses are provided from the same numerical weather prediction (NWP) model system as operational forecasts from the Met Office [D. Walters, et al., "Enhancing Vertical and Horizontal Resolution in the Met Office Global NWP (Unified) Model, in preparation]; the same fields are provided, but on a 0.375° latitude by 0.5625° longitude grid, at 27 levels from 1000 to 0.4 hPa (to 0.1 hPa starting in May 2007). When there is a need to distinguish, the recent MetO analyses are referred to as MetO-NWP and the original ones developed for UARS as MetO-STT. DMPs are calculated for all instruments from the MetO data.

The GEOS-4 analyses are described by *Bloom et al.* [2005]; a Physical Space Statistical Analysis Scheme is used. The GEOS-4 data used here are provided on 55 hybrid (σ/pressure) model levels from the surface to 0.01 hPa. The horizontal grid is 1.0° latitude by 1.25° longitude. six-hourly average fields are provided centered at 0, 6, 12 and 18 UT. Besides the standard meteorological variables, GEOS-4 products include an extensive set of fields from the model and assimilation system, including PV calculated internally in the model. DMPs for ACE-FTS and for MLS v1.5 data are calculated from GEOS-4.

GEOS-5 analyses [*Reinecker et al.*, 2007] have been produced for the full period of the Aura mission, and have replaced GEOS-4 as the operational system. GEOS-5 uses the Gridpoint Statistical Analysis method of *Wu et al.* [2002], a 3D-Var system, with a six-hour analysis window. Analyses are produced for surface pressure, temperature, winds, moisture and ozone. Along with operational meteorological products, infrared radiances from AIRS on EOS-Aqua were assimilated, as described in detail by *Stajner et al.* [2007]. The interface between the observations and the GCM is performed using the incremental analysis update (IAU) approach [*Bloom et al.*, 1996], which avoids shocking the model, thus producing smoother analyses. GEOS-5 analyses are provided on 72 model levels from the surface to 0.01 hPa, and a 0.5° latitude by 2/3° longitude grid. DMPs for ACE-FTS and for MLS v2.2 data are calculated from GEOS-5.

NCEP/CPC analyses (used for SAGE II DMPs) are from an objective analysis at levels above 10 hPa (above 100 hPa prior to April 2001) [*Finger et al.*, 1965, 1993; *Gelman et al.*, 1986, 1994]; these analyses have been available since June 1979. Analyses at and below 100 hPa are from the tropospheric analysis and forecast cycle [e.g., *Derber and Wu*, 1998; *McNally et al.*, 2000]. The NCEP data are provided once a day at 12UT on a 65×65 point polar stereographic grid for each hemisphere; the fields used here are interpolated to a 2.5°×5° latitude/longitude grid. Only temperature and geopotential height are provided in the stratosphere, so horizontal winds are calculated from the NCEP geopotential heights using a form of the primitive equations that neglects the vertical advection and time tendency terms [*Randel*, 1987; *Newman et al.*, 1989].

3. DMP Field Description

Table 1 lists the DMPs calculated for the solar occultation instruments; these DMPs are produced on the vertical grids used for the solar occultation instruments' data. Table 2 lists the DMPs provided for the MLS instrument. MLS records over 100 times more profiles per day than the solar occultation instruments, so calculating the DMPs is computationally intensive. To make the calculations feasible, and since the MLS positions are not altitude-dependent, MLS DMPs are calculated and output on standard θ or pressure levels, allowing the calculations to be done in advance on the gridded meteorological analysis fields once for each analysis time, and then interpolated to the MLS times and positions. File formats and access to the DMPs are described in the Appendix; the DMP calculations are described in more detail below.

3.1. Description of Calculations and Interpolations

Interpolation of fields provided in the meteorological analyses (horizontal winds, temperature, geopotential height, PV from GEOS-4 and GEOS-5 analyses) is done linearly in time (between six-hourly fields for the GEOS analyses, daily fields for the MetO analyses) and bi-linearly in latitude and longitude. Vertical interpolations are linear in $\log(\theta)$ for PV or log(pressure) for the other products. EqL is calculated on isentropic surfaces and interpolated linearly in $\log(\theta)$. For the MetO and NCEP DMPs, PV is calculated as described by *Manney et al.* [1996b], based on the algorithm of *Newman et al.* [1989]; PV is provided from the assimilation model in the GEOS datasets, and these PV fields are used in the DMP files, as it is more fully consistent with the analyzed fields than an offline calculation. Scaled PV (sPV) is in "vorticity units" [10^{-4} s^{-1}, *Dunkerton and Delisi*, 1986; *Manney et al.*, 1994b], giving a similar range of values at levels throughout the stratosphere.

Horizontal PV gradients are calculated on isentropic surfaces and normalized to the hemispheric average; the calculation is strongly dependent on the resolution of the meteorological analysis used. The magnitudes of gradients calculated from different meteorological analyses are thus not directly comparable. Horizontal temperature gradients are calculated on pressure levels. LOS PV and temperature gradients are also provided for several of the solar occultation instruments for which the LOS angle information is available. These are potentially useful for validation and data

Table 1. Derived Meteorological Product (DMP) Fields and Units for Solar Occultation Instruments

Field	Units	Description
Geolocation (from Instrument Geometry)		
Alt	km	(2D[1]) Altitudes
Lat	deg	(2D) Latitudes as a function of Altitude
Lon	deg	(2D) Longitudes as a function of Altitude
Sun Dir[2]	deg cw from N	(2D) Line-of-Sight angle (LOS)
Interpolated from Meteorological Data		
Temperature	K	(2D) Temperature from meteorological data
Geop Hgt	m	(2D) Geopotential Height
Zonal Wind	m/s	(2D) Zonal Wind
Merid Wind	m/s	(2D) Meridional Wind
Calculated from Meteorological Data		
θ	K	(2D) Potential Temperature from met data
PV[3]	10^{-4} K m^2 kg^{-1} s^{-1}	(2D) Potential Vorticity (PV)
Scaled PV	10^{-4} s^{-1}	(2D) Scaled PV, in "vorticity units"[4]
EqL	deg	(2D) Equivalent Latitude (EqL)
Hor PV Grad	–	(2D) Normalized horizontal PV gradient
Hor T Grad	K/km	(2D) Horizontal temperature gradient
LOS T Grad[2]	K/km	(2D) Temperature gradient along LOS
LOS PV Grad[2]	(10^{-4} K m^2 kg^{-1} s^{-1})/km	(2D) PV gradient along LOS
EqL - VEC	deg	(2D) Distance (EqL) from vortex edge center
EqL - VEI	deg	(2D) Distance (EqL) from inner vortex edge
EqL - VEO	deg	(2D) Distance (EqL) from outer vortex edge
Dyn Tropopause	km	(1D[1]) Dynamical tropopause altitude[5]
TG Tropopause	km	(1D) WMO tropopause altitude

[1] 2D indicates profile information, 1D a single value for each occultation
[2] Not Available for ACE or HALOE DMPs
[3] Interpolated directly from provided dataset for DMPs derived from GEOS-4
[4] *Dunkerton and Delisi* [1986]; *Manney et al.* [1994b]
[5] 3.5 PVU joined to 380 K θ in tropics, see text

Table 2. Derived Meteorological Product (DMP) Fields for MLS

Field	Units	Description
On Standard Pressure Surfaces		
Pressure	hPa	Standard Pressure Level Values
θ	K	Potential Temperature from met data
Geop Hgt	m	Geopotential Height
On Standard Potential Temperature Surfaces		
θ	K	Standard θ level values
Pressure	hPa	Pressure on θ surfaces
Zonal Wind	m/s	Zonal Wind
Merid Wind	m/s	Meridional Wind
PV	10^{-4} K m^2 kg^{-1} s^{-1}	Potential Vorticity (PV)
EqL	deg	Equivalent Latitude (EqL)
Hor PV Grad	–	Normalized horizontal PV gradient
EqL - VEC	deg	Distance (EqL) from vortex edge center
EqL - VEI	deg	Distance (EqL) from inner vortex edge
EqL - VEO	deg	Distance (EqL) from outer vortex edge
Single-Level Fields		
Latitude	deg	MLS Level 2 reported latitude
Longitude	deg	MLS Level 2 reported longitude
Dyn Tropopause	hPa	Dynamical tropopause pressure
TG Tropopause	hPa	WMO tropopause pressure

quality studies in assessing the homogeneity of atmospheric conditions along the LOS.

Knowledge of the position of measurements with respect to the vortex edge frequently aids in interpretation, and can be valuable for selecting observations from the same air mass [e.g., *Nassar et al.*, 2005; *Sica et al.*, 2007]. To provide this information in the DMP files, the vortex edge "center" is defined as the EqL of the maximum of the windspeed times the PV gradient. The "inner" and "outer" vortex edges are EqL on vortex and extravortex sides, respectively, where that vortex definition function changes curvature [e.g., *Nash et al.*, 1996]. The vortex is undefined if $\theta < 345$ K, or if: The EqL of the vortex edge center is greater than 80° [vortex too small, e.g., *Manney et al.*, 1994a], the windspeed is less than 15.2 m/s [polar night jet is too weak, e.g., *Nash et al.*, 1996], or the normalized PV gradient is less than 1.1 (not significantly above average).

Figure 1 shows the windspeed, PV gradient, and position in relation to the vortex edge center from MLS GEOS-4 DMPs during northern hemisphere (NH) winter and spring. Only those days on which a vortex edge is defined can be included in the averages for the position relative to the vortex edge; thus, in some cases (e.g., SH lower stratosphere in March, when vortex is just starting to develop and does so substantially over the month) a vortex edge is defined when the plotted PV gradients and windspeeds do not show an obvious transport barrier. The vortex appears to be defined in the SH at the lowest levels in January in Figure 1, a mis-identification of the top of the upper tropospheric subtropical jet as the vortex edge; this is a common occurrence, but setting the lower θ limit to a higher value would eliminate much of the SH subvortex region in winter and spring. In the upper stratosphere, and near the stratopause, the jet/PV gradient structure is much more complex, and thus mis-identification (e.g., January in SH) is common; in fact, there is often not a single most appropriate definition of the upper stratospheric vortex edge, even in winter.

The inclusion of windspeed in the definition reduces the likelihood of spurious maxima in the PV gradient at high EqL being identified as the vortex edge, and the use of the combined function provides a means for choosing which of multiple peaks in the and PV gradient [common in fall, e.g., *Manney et al.*, 2002] are selected. Automated vortex edge identification is most robust under conditions for which the vortex is simply defined, i.e., when there is a single region of strong PV gradients associated with a sharply peaked polar night jet. This is the case in the middle to lower stratosphere during SH winter and many NH winters; in these cases, results from the algorithm used for the DMPs agree closely with those using the criteria of *Nash et al.* [1996] and other methods of determining the vortex edge. Our comparisons suggest that the algorithm used for the DMPs can give more desirable results than the *Nash et al.* [1996] method in complex situations such as that in the upper stratosphere.

Figure 2 shows the vortex edge as a function of time, versus sPV and ACE-FTS CH_4, for December 2004 through

March 2005, in the upper and lower stratosphere; since CH_4 is a long-lived tracer with strong gradients across the vortex boundary, it is strongly negatively correlated with sPV throughout the stratosphere [*Manney et al.*, 1999, and references therein]. In the lower stratosphere (through the middle stratosphere, not shown), the vortex edge is marked by a very well defined region in sPV and CH_4 (and other trace gases and dynamical markers, not shown) in January through late March, becoming slightly less distinct only after mid-March during the early final warming. In the upper stratosphere, however, the region of the vortex edge is much less well defined throughout the winter because of its complex structure, and Figure 2 shows a less distinct transition in CH_4 and sPV. These results demonstrate that caution should be used in applying automated vortex edge identification methods, and their appropriateness should be checked against the physical conditions. For individual profile comparisons, or other studies where it is critical to correctly identify the air mass properties of each measurement, it is suggested that the vortex edge criteria be compared with sPV, PV gradients, and windspeeds; where DMPs are available from different meteorological analyses, comparison of these fields can also aid in assessing the robustness of identification of position with respect to the vortex.

The conditions under which any automated vortex edge identification is robust are exactly those under which any reasonable definition of the vortex edge (including, e.g., a specific sPV contour) will provide a comparable value. For the vortex averages shown below (section 3.2), an sPV contour (1.4×10^{-4} s^{-1}) is used, chosen by visual inspection to be within the region of strong PV gradients throughout the stratosphere; this definition, or nearby sPV values, has been used extensively in previous studies [e.g. *Manney et al.*, 1994a, b, 2003a; *Jin et al.*, 2006b]; similar results are obtained using the EqL from the vortex edge center, though these depend more strongly on which meteorological analyses is used for the vortex edge calculation.

The WMO (temperature gradient) tropopause height is defined as the lowest altitude where the temperature lapse rate drops below 2 K/km and remains below that for at least 2 km. The WMO tropopause is calculated using the algorithm of *Reichler et al.* [2003]. For the solar occultation instruments, it is calculated from the meteorological analyses' temperatures after they have been interpolated to the solar occultation instrument's measurement location and vertical grid; for MLS it is calculated on the native grid of the meteorological analysis before interpolating to the MLS times/positions. The "dynamical" tropopause is defined by the 3.5×10^{-6} K m^2 kg^{-1} s^{-1} PV contour in the extratropics (found to be an appropriate values by, e.g., *Highwood and Berrisford* [2000] and *Schoeberl* [2004]), joined to the 380 K isentropic surface in the tropics or subtropics where that PV contour rises above this level. Tropopause altitude is saved for the solar occultation instruments, and tropopause pressure for MLS, consistent with the native vertical grid of each satellite dataset. Because of the limited vertical resolution of the meteorological analyses, the calculations used here (especially the WMO tropopause where the calculation of vertical gradient changes depends on resolution) are not expected to be able to capture very fine vertical structure that often exists near the tropopause and can alter local tropopause levels [e.g., *Birner et al.*, 2002]. Figure 3 shows the WMO and dynamical tropopause altitude for MLS and the five solar occultation instruments during January 2005. The WMO and dynamical tropopause calculations agree quite well in the summer hemisphere through midlatitudes in the winter hemisphere; as noted previously [*Highwood and Berrisford*, 2000, and references therein], there is often a deep, nearly isothermal layer in the polar winter where the WMO tropopause is not well defined. At the latitudes covered by the solar occultation instruments, the range of tropopause values sampled is typically similar to that sampled by MLS; more MLS values in the low end of the range may simply reflect inaccuracy in the conversion of the MLS tropopause location from pressure to altitude.

3.2. Sampling Issues

The DMPs help us to explore the effects of sampling and coverage on a variety of comparisons and analyses of the satellite data by providing versions of the same fields as sampled by different instruments.

An example of how the MLS sampling may affect our perception of atmospheric conditions is given in Figure 4, showing PV from the 1x1.25° GEOS-4 analyses in the lower and upper stratosphere, and maps of the same fields gridded from the MLS GEOS-4 DMPs. (MLS fields are mapped on a 2x5° grid using a weighted average of all the points in a day within a specified distance of the gridpoints.) The day shown is a case where the MLS sampling captures some small scale features quite well, e.g., the intrusion into the vortex near 30°E at 490 K, and the very narrow double filament drawn off the vortex near 120–180°E, 30°N at 1700 K. However, much of the small-scale structure inside the vortex at 1700 K is either distorted or not apparent in the MLS DMP fields, and other small-scale features are smeared out (e.g., the small high/low PV dipole near 310°E, 30°N at 490 K). When comparing features in PV with MLS trace gas observations, viewing the PV fields as sampled by MLS can help assess whether features in the full PV fields may be missed or distorted by the MLS sampling.

With the sparse coverage and varying views of the solar occultation instruments, sampling effects are always an

important consideration. Figure 5 shows the latitude and sPV sampled by each of the solar occultation instruments as a function of EqL in the lower stratosphere during the 2004-2005 NH winter. The broad range of EqL covered each day based on measurements at a single geographic latitude demonstrates the power of an EqL view in describing the full range of atmospheric conditions using solar occultation data; however, differences in sampling still argue for continued caution in interpretation of these measurements. The vortex edge is near 1.3-1.5$\times 10^{-4}$ s^{-1} sPV at this time and level (region of strong sPV and tracer gradients, cf. Figure 2). HALOE and SAGE II sampled very little vortex air during the winter; SAGE II coverage moved into the vortex in late February, when variability in vortex shape and position increased [e.g., *Manney et al.*, 2006]. Its measurements in late March reached the highest EqLs; despite being taken at much lower geographical latitudes than those of the other instruments sampling the vortex at this time ($\sim$55–65° as opposed to $\sim$68–85°), the highest sPV values sampled by SAGE II were comparable to those seen by ACE, POAM III, and SAGE III, suggesting that at this time the geographical latitude should not be a large factor in comparing fields that are well-correlated with the vortex. The four instruments that measured primarily at high latitudes (ACE (ACE-FTS and MAESTRO), POAM III, SAGE III) also covered high EqLs with measurements at quite different geographic latitudes. In January and February, SAGE III's denser coverage (resulting from reduced sampling for POAM III and limited data downlink time for ACE, section 2.1) and higher-latitude sampling result in measurements at higher sPV values and more complete coverage of the regions of very strong sPV gradients than provided by ACE and POAM III. These differences can be a significant factor in some comparisons. Different coverage will also, of course, be a large factor in comparisons of fields that do not correlate well with the vortex, e.g., temperature (section 4.3), O_3 in some regions (section 4.2), and some trace gases affected by polar processing (section 4.3).

The wide variation in density and completeness of vortex coverage (Figure 5) strongly influences interpretation of vortex-averages from different instruments. Figure 6 shows the average latitude of all measurements inside the vortex (defined by the 1.4 $\times 10^{-4}$ s^{-1} sPV contour, cf. Figure 2, section 3.1) during the NH 2004-2005 fall and winter, from MLS and ACE measurements. As expected, MLS average latitudes are typically from $\sim$65° to $\sim$72°N (except at lowest levels where vortex is smaller); they decrease dramatically during the vortex breakup starting in early March as the vortex and its remnants move away from the pole. In contrast, the latitude from solar occultation instruments (represented here by ACE) is determined solely by their measurement patterns. Figure 7 shows how these sampling differences can affect interpretation of vortex averages of trace gases. Vortex averages of the long-lived species N_2O, H_2O, and CO are shown in the 2004-2005 NH fall and winter from ACE-FTS and MLS v1.5 (v1.5 is used to show the time evolution throughout the season, including periods when v2.2 MLS data are not yet available) data, along with similar averages using only those MLS measurements that are coincident with ACE observation locations. For the "colocated" MLS averages, coincidence criteria are $\pm 1^\circ$ latitude, $\pm 8^\circ$ longitude, and 12 hours, similar to values used in traditional coincident comparisons in other papers in this special issue; results do not depend strongly on the exact coincidence criteria, and depend especially weakly on the longitude criterion.

Strong descent from the mesosphere through the middle stratosphere is generally represented well in both datasets, with the ACE-FTS capturing the extent and timing of CO and H_2O changes. After $\sim$15 January, the magnitude of changes in N_2O and H_2O in the lower to middle stratosphere is correctly estimated by ACE-FTS. However, during November through early January (across the gap in ACE data), ACE-FTS and MLS vortex averages do not agree well. At this time, mixing into the vortex resulting from strong wave activity led to increases (decreases) in vortex-averaged N_2O (H_2O) in the middle and lower stratosphere, and a pause in the descent of high CO/low H_2O contours in the upper stratosphere. When MLS is sampled like ACE, a significant overestimate of the N_2O and H_2O changes in the middle and lower stratosphere results because ACE sampled near the edge of the vortex at this time, where N_2O (H_2O) is higher (lower) and mixing in of extra-vortex air is greater. The co-located MLS averages agree very well with those from ACE-FTS. ACE-FTS vortex-averaged values converge with those from MLS when ACE sampling moves farther into the vortex in late January. In late November, ACE-FTS and the colocated MLS averages also show a decrease (rather than just a pause in the increase in full MLS averages) in CO in the upper stratosphere, resulting from the same sampling effects. "Vortex-averages" from solar occultation instruments are often used to estimate descent rates for polar processing and O_3 loss studies [e.g., *Nassar et al.*, 2005; *Jin et al.*, 2006b] – situations such as this could lead to a substantial overestimate of descent from ACE-FTS measurements after the period of strong mixing.

The vortex averages shown above illustrate a type of analysis for which a vortex-centered view is still highly dependent on the latitude sampling of the individual instruments. For other types of analyses, using DMP products to analyze measurements taken in similar air masses can facilitate more comprehensive comparisons and detailed scientific studies as a function of the meteorological conditions under which

the measurements were taken. In the following section, we provide examples of comparisons of MLS and solar occultation data using the DMPs during polar winter. These examples illustrate situations in which the degree of correlation with the vortex of atmospheric processes affecting various species determines how robust the comparisons between instruments with different sampling are. Our aim is neither to present a comprehensive validation of MLS versus solar occultation data (though our examples complement detailed analyses given in other papers for this special issue), nor to provide detailed scientific analysis, but rather to illustrate the value of the DMPs as well as precautions that still need to be taken to ensure consistent analyses when combining datasets with disparate sampling patterns.

4. Comparisons of MLS with Solar Occultation Data Using DMPs

In the following subsections, we compare EqL/time series and EqL/θ vertical sections of MLS v2.2 and solar occultation data. Comparisons that involve only ACE-FTS and MLS use EqL and θ from the GEOS-5 DMPs, others use MetO DMPs. EqL/θ plots are produced by taking weighted averages around each gridpoint in EqL, θ and uncertainty, as described by *Manney et al.* [1999, 2001]. The EqL grid spacing used is 5°, so many MLS points are included in the average for each gridpoint. The θ grid corresponds to an ∼3-km spacing, comparable to the vertical resolution of many of the instruments, and coarser than the data grids. EqL/θ plots are for data from continuous 7–8-day periods. MLS/ACE-FTS comparisons are shown to the higher altitudes allowed by the GEOS-5 DMPs (section 2.3).

EqL/time plots are produced in the same way, but are gridded in time instead of θ. Time gridpoints are at 12 UT each day. Plots for the solar occultation instruments have a 5° latitude half-width and 3-day time half-width; 2.5° latitude and 1.5 day time half-widths are used for MLS to more fully illustrate potential sampling effects on the representation of time evolution.

4.1. Long-lived Tracers

Three species measured by MLS that are commonly used as tracers of transport are N_2O, H_2O, and CO. The vortex averages in Figure 7 (section 3.2) showed good agreement of ACE-FTS with coincident MLS v1.5 measurements of CO and H_2O in most regions, but slightly lower MLS H_2O near the stratopause. N_2O showed excellent qualitative agreement in time evolution, but a slight low bias in MLS with respect to ACE-FTS, as was noted for NH means of coincident profiles by *Froidevaux et al.* [2006]. V2.2 MLS N_2O is on average about 10% higher than v1.5 between 46 and 2 hPa [*Lambert et al.*, 2007, this issue], which reduces (though does not eliminate, see below) that bias.

Figure 8 shows times series as a function of EqL at 490 K (∼18 km, in the lower stratosphere) of MLS v2.2 and ACE-FTS N_2O and H_2O. Very good qualitative agreement is seen in the time evolution of both species. Both species show slightly weaker PV gradients across the vortex edge (region of strongest gradients, solid sPV contours and contour just below them) in ACE-FTS than in MLS, leading to slightly lower (higher) N_2O (H_2O) values outside the vortex. This results primarily from the incomplete sampling of ACE in that region (e.g., Figure 5, section 3.2), though MLS v2.2 N_2O does show a small high bias with respect to ACE-FTS throughout the lower stratosphere [*Lambert et al.*, 2007, this issue]. MLS H_2O and N_2O are both substantially lower in the vortex core than ACE-FTS values. Since both the horizontal and vertical gradients of the two species are opposite, dependence on sampling in either coordinate would tend to produce opposite biases in H_2O and N_2O, suggesting that the vortex-core difference results from real biases between the instruments. The slight low bias in the MLS N_2O in the lower stratosphere is consistent the results of *Lambert et al.* [2007, this issue]. In the middle stratosphere (not shown), MLS and ACE-FTS H_2O and N_2O time evolution agrees well quantitatively. POAM III H_2O (not shown) is noisier than MLS and ACE-FTS, and displays some artifacts; nevertheless, very similar time evolution is seen in the middle and lower stratosphere, but with values biased high with respect to MLS and ACE-FTS.

EqL/θ sections of MLS and ACE-FTS N_2O are shown in Figure 9 for the NH in March. These show the persistent low bias of MLS in the polar vortex, and in the summer polar lower stratosphere. Similar plots using only the MLS data coincident with ACE-FTS (not shown) have only slightly smaller biases in the lower stratosphere, indicating that sampling differences are not the primary factor producing this pattern. *Lambert et al.* [2007, this issue] also show a low bias in this region in hemispheric averages of differences between MLS and ACE-FTS coincident profiles. Elsewhere, localized differences are up to ∼15 ppbv, but most areas are within ∼5 ppbv, with ACE-FTS slightly lower than MLS.

Figure 10 shows EqL/θ comparisons of MLS v2.2 H_2O with ACE-FTS and HALOE during March 2005. MLS and ACE-FTS agree extremely well throughout the range, with differences typically under 0.2 ppmv (less than 5%) and maximum localized differences up to 15%. MLS is higher than HALOE by ∼0.2–1.0 ppmv (∼5–25%) throughout the range shown, consistent with HALOE H_2O biases reported elsewhere [e.g., *Kley et al.*, 2000; *Lambert et al.*, 2007, this issue]. SAGE II and POAM III H_2O EqL/θ-mapped fields for this period (not shown) are noisy, but comparisons indi-

cate that SAGE II is ∼5–15% lower than MLS between 500 and 1600 K, and POAM III is ∼5–15% higher than MLS between 400 and 1600 K. Each of these biases is consistent with hemispheric biases with respect to v1.5 H_2O data in *Froidevaux et al.* [2006]; *Lambert et al.* [2007, this issue] show little overall bias between v1.5 and v2.2 H_2O in the stratosphere.

The chemical lifetime of CO varies from a few weeks to many months, making it a useful tracer of transport [e.g., *Solomon et al.*, 1985; *Allen et al.*, 1999] in many situations. As shown in Figure 7 (section 3.2), starting in fall very high CO descends from the mesosphere into the winter stratospheric vortex. Figure 11 shows the time evolution of MLS v2.2 and ACE-FTS CO in the upper stratosphere. Quantitative agreement between ACE-FTS and MLS is good, as is also the case in the middle stratosphere (not shown). The combination of sparse sampling and longer time averaging used in the EqL/time gridding for ACE-FTS are the primary factors responsible for the small qualitative differences in short-lived features near the vortex edge in late January and early February. Consistent with the good agreement shown here, *Pumphrey et al.* [2007, this issue] show little overall bias between ACE-FTS and MLS stratospheric CO, but some remaining vertical oscillations in MLS CO in the stratosphere that can result in biases at individual levels.

Figure 12 shows an EqL/θ comparison of MLS v2.2 and ACE-FTS CO for March 2005. The MLS CO measurement is noisy, as seen in the variations in mid-EqLs in the upper stratosphere, and v2.2 still shows some remaining vertical oscillations in the stratosphere [*Pumphrey et al.*, 2007, this issue]; because of this, and the extremely large range of CO values, difference plots (not shown) are difficult to interpret. However, qualitative agreement is good throughout the range. Quantitative agreement is best in the Arctic lower mesosphere, above about 2000 K (50 km). A high bias of MLS with respect to ACE-FTS in most regions, but low bias from ∼600 to 800 K, is consistent with profile comparisons shown by *Pumphrey et al.* [2007, this issue]. MLS is strongly biased high with respect to ACE-FTS at the lowest levels shown, in the upper troposphere/lower stratosphere, consistent with the results of *Livesey et al.* [2007a, this issue].

The effects of disparate sampling on interpretation of these long-lived tracer fields are minimal, and easily assessed using the DMPs (e.g., using sPV fields to diagnose the representation of gradients across the vortex edge). Using DMPs for mapping in EqL to provide a vortex-centered view is thus a powerful method for combining datasets with different sampling patterns to enhance validation and scientific studies; for the latter, EqL mapping can be used to analyze long-lived tracers that are not measured by MLS (e.g., CH_4 from ACE-FTS) in a consistent framework with the species shown here.

In the following subsections, we examine other species for which chemical and other processes not correlated with the vortex may make some analyses in EqL coordinates more challenging.

4.2. Ozone

In the lower stratosphere, the chemical lifetime of O_3 is long, except in the cold polar winter when heterogeneous chemical processing occurs [e.g. *Solomon*, 1999]. Figure 13 shows a comparison of lower stratospheric O_3 from MLS and solar occultation instruments with good coverage of the vortex during the 2004-2005 NH winter. 2004-2005 was arguably the winter with the largest lower stratospheric chemical O_3 loss of any NH winter [*WMO*, 2007, and references therein]. The morphology of O_3 was also complex, being highest near the vortex edge even before chemical loss began; this distribution complicates separation of dynamical and chemical effects and makes assessment of chemical O_3 loss more problematic [e.g., *Manney et al.*, 2006]. O_3 evolution in the vortex and along its edge agrees quite well between MLS, ACE-FTS, MAESTRO, POAM III, and SAGE III. The discontinuity in MAESTRO O_3 between ∼10 and 20 January (seen most strongly near the vortex edge) is an artifact related to the time offset from ACE-FTS at specific measurement times (section 2.1.2). POAM III and SAGE III show slightly higher values at 40–60°EqL than MLS, SAGE II and HALOE; this may be related to sampling, as the POAM III and SAGE III measurements are all taken at higher latitudes (Figure 5) where high O_3 values are not completely aligned with the vortex [see, e.g., maps in *Manney et al.*, 2006]. ACE-FTS vortex interior values are slightly higher overall ($\lesssim$0.2 ppmv) than those from the other instruments, but with very similar time evolution. Examination of late-January/mid-March differences as a function of EqL and θ (not shown) from solar occultation instruments and MLS v2.2 data indicates very similar amounts of decrease in the lower stratospheric vortex (a signature of chemical loss), a maximum of ∼1.0±0.1 ppmv, for each instrument, near 70°EqL and 490 K. Detailed calculations [*Singleton et al.*, 2007] using MLS v1.5 for this winter showed very good agreement in O_3 loss estimated from these instruments, especially when MLS v1.5 data were sampled similarly to the solar occultation instruments; values for chemical O_3 loss were larger than the observed changes reported here due to replenishment of O_3 by diabatic descent [*WMO*, 2007, and references therein].

O_3 at tropopause level is also primarily controlled by dynamics; since O_3 gradients across the tropopause are extremely strong, O_3 is sometimes used to identify the

tropopause [e.g., *Bethan et al.*, 1996]. Figure 14 shows O_3 at the tropopause from MLS v2.2 data and five solar occultation instruments for 18-day periods in January–February and September 2005. Given the strong O_3 gradients, this is a very sensitive comparison; also, in this region of very low O_3 and increasing possibility of clouds, the retrievals are difficult. Overall, the values agree remarkably well, especially considering that measurements at the same latitude from different instruments may have been taken several days apart. Most of the instruments show some points with negative O_3, reflecting the difficulty of retrieving such low O_3 values (negative MLS values represent a very small fraction, $\sim$1.7–4.2%, of the total number of MLS values, and are concentrated in the tropics for the WMO tropopause (where O_3 is lowest and clouds most likely to affect the retrievals) and in the polar winter (where atmospheric variability is greatest) for the dynamical tropopause). The vast majority of O_3 values at the dynamical tropopause from all instruments are $\sim$0.1 to 0.4 ppmv, consistent with previous estimates [e.g. *Bethan et al.*, 1996; *Pan et al.*, 1997]. The MLS average at the dynamical tropopause, near 0.15 ppmv, agrees well with the center of the distributions for ACE-FTS, POAM III and SAGE III, and is slightly higher than that for HALOE and MAESTRO. O_3 varies more at the WMO tropopause, and shows a very large scatter in the winter polar regions, where that definition of the tropopause is most ambiguous (e.g., Figure 3); MLS, ACE-FTS, MAESTRO, and SAGE III all show large ($\sim$2.0 ppmv) values at high northern latitudes in January/February, when the temperatures and tropopause height were highly variable [e.g. *Schoeberl et al.*, 2006]; a similar plot for March 2005 (not shown), when the WMO tropopause is better defined, shows much lower, more typical, values in the Arctic. A very similar pattern is seen in the Antarctic winter, but with less scatter in the O_3 values for all instruments, likely due to more symmetric conditions in the SH winter resulting in more uniform sampling.

Figures 15 and 16 compare v2.2 MLS O_3 with each of the solar occultation instruments during March 2005. First, Figure 15 shows MLS O_3 mapped in EqL/θ using the GEOS-5 and the MetO DMPs, and the difference between them; this demonstrates that the differences in gridding from using different DMPs are small compared to differences seen below between instruments. ACE-FTS and MAESTRO comparisons in Figure 16 use GEOS-5 DMPs and extend to higher levels; other comparisons use MetO DMPs for MLS as well as the solar occultation instruments.

Figure 16 shows very good agreement between all instruments in the lower stratosphere and around the tropopause; differences are typically less than 0.2 ppmv, and, even at these low O_3 values, less than $\sim$5%. An exception is a slight high bias of MLS with respect to HALOE at NH midlatitudes near 20 km, consistent with previously reported biases between HALOE and SAGE II [e.g., *Morris et al.*, 2002]; *Jiang et al.* [2007, this issue] and *Froidevaux et al.* [2007b, this issue] also show some evidence (albeit inconclusive) of a small high bias in MLS v2.2 O_3 at the lowest retrieval levels. MLS also shows a slight low bias with respect to ACE-FTS at the lowest levels shown near $\pm$40°EqL, at the edges of the ACE-FTS coverage.

Good agreement between MLS and the solar occultation instruments in O_3 mapped using DMPs from the tropopause through the lower stratosphere (Figures 13, 14, and 16) is consistent with the dominance of transport processes (or, in the polar winter, chemical processes that are generally well-correlated with the vortex) in controlling the O_3 distribution. At higher altitudes, O_3 chemical lifetimes decrease, and the situation becomes more complex.

In the middle to upper stratosphere ($\sim$900–1600 K) above $\sim$40°EqL, Figure 16 shows that MLS is higher than ACE-FTS, POAM III and SAGE III (high-latitude-sampling instruments) and lower than SAGE II and HALOE (low-latitude-sampling instruments). MLS is higher than MAESTRO (with same sampling as ACE-FTS, with sunset profiles in the NH and sunrise profiles in the SH at this time) from $\sim$900 to 1300 K, above which a substantial high bias in sunset MAESTRO profiles with respect to SAGE III and POAM III has been reported [*Kar et al.*, 2007]. This is the region where "low-O_3 pockets" [*Manney et al.*, 1995b; *Harvey et al.*, 2004] are common: High O_3 from low latitudes is drawn into and trapped in the anticyclone for many days. When thus confined at high latitudes, O_3 relaxes chemically toward the lower equilibrium values for these latitudes (whereas air outside the anticyclones is continually being mixed with higher-O_3 air from low latitudes) [*Morris et al.*, 1998; *Nair et al.*, 1998]. The pattern seen in MLS data (Figure 15), with highest values apparently excluded from this EqL band, is characteristic of the morphology seen when a low-O_3 pocket is present [e.g., *Manney et al.*, 1999, 2001]. Low-O_3 pockets were observed continuously from early December 2004 through late March 2005, and were sampled by MLS and all solar occultation instruments examined here [*Harvey et al.*, 2007]. A detailed discussion of effects of sampling on low O_3 in the anticyclones as observed by MLS and the solar occultation instruments, and discussion of potential pitfalls in using EqL coordinates for this type of analysis, is given by *Harvey et al.* [2007]. EqL/θ comparisons like those in Figure 16 constructed using only MLS observations coincident with the solar occultation instruments (not shown) reduce the differences in the middle stratosphere to less than $\sim$0.4 ppmv, and in some cases change the sign (e.g., MLS is slightly lower than ACE-FTS in this region), conclusively demonstrating that these differ-

ences result from the interplay of sampling, transport and chemistry in this region.

In the upper stratosphere (and lower mesosphere for ACE-FTS, above ~1600 K, ~45 km), Figure 16 shows MLS O_3 to be low with respect to ACE-FTS and SAGE III; this difference is global and persistent across the time periods examined. Similar differences were seen by *Froidevaux et al.* [2006] for MLS v1.5 comparisons with ACE-FTS v2.1 data; *Walker et al.* [2005] also noted that ACE-FTS v1.0 O_3 was high with respect to other instruments from about 40 to at least 60 km, and this difference persists in ACE-FTS v2.2 O_3 update data. MAESTRO is also high in this region, consistent with the sunset occultation biases reported by *Kar et al.* [2007]. *Froidevaux et al.* [2007b, this issue] show a few percent increase in MLS v2.2 over v1.5 in the upper stratosphere, with a continuing low bias (by ~5–10%) with respect to ACE-FTS v2.2 data. The high bias of MLS with respect to ACE-FTS in the lower mesosphere above ~3000 K is also persistent across the periods examined, and consistent with the results of *Froidevaux et al.* [2007b, this issue]. Thus, although O_3 chemical lifetimes are short in the upper stratosphere, raising the possibility of sampling issues arising from chemical processes not well correlated with the vortex, the biases seen here are consistent with those reported in traditional coincidence analyses.

The preceding discussion of O_3 indicates overall very good agreement between MLS and all of the solar occultation instruments studied when viewed with respect to EqL, but highlights sampling issues that are important in interpretation of sparse measurements. Mapping in EqL is very valuable in scientific studies with SO data, allowing examination of the full range of conditions sampled and averaging of air from similar air masses; the above results show it to be a valuable tool for O_3 from the tropopause through the lower stratosphere. At higher levels, chemical processes that are not well correlated with the vortex can complicate the interpretation of EqL-mapped O_3.

4.3. Other Fields

4.3.1. HNO_3 HNO_3 in the middle and lower stratosphere is often well-correlated with the vortex, but situations do occur for which the sparse sampling of solar occultation instruments can lead to apparent disagreements with MLS. In the middle stratosphere (Figure 17), qualitative time evolution appears generally consistent between MLS and ACE-FTS, with lower overall MLS values in agreement with the results of *Santee et al.* [2007c, this issue]. The low MLS HNO_3 regions inside the vortex and along the vortex edge in January and February provide an illustrative example of differences related to the sparse ACE-FTS sampling. Maps of MLS 850 K HNO_3 during this period (Figure 18) show the evolution of a partial band of low HNO_3 just inside the vortex edge. ACE-FTS observation locations are overlaid, and show that ACE-FTS typically measured near the edge of this low HNO_3 region where values were slightly higher; this pattern, and the three-day time half-width used for the ACE-FTS gridding, result in a faint and smeared echo of the feature in the ACE-FTS data.

In the lower stratosphere, HNO_3 is critical in both the activation and the deactivation of chlorine, and thus indirectly regulates O_3 destruction [*Solomon*, 1999; *Santee et al.*, 2004, and references therein]. The time evolution of MLS v2.2 and ACE-FTS HNO_3 as a function of EqL in the lower stratosphere (not shown) agrees quite well, but ACE-FTS misses some of the lowest values in the vortex indicative of sequestration in PSCs. EqL/θ comparisons of MLS v2.2 and ACE-FTS HNO_3 in January 2005 (Figure 19), during a period of strong PSC activity [*Jin et al.*, 2006a], show good qualitative agreement, including the position and morphology of the primary HNO_3 peak and a secondary peak in the polar winter upper stratosphere (~900-1300 K) that is a common feature of the HNO_3 distribution [e.g., *Orsolini et al.*, 2005a]. Quantitative agreement is fairly good in the levels surrounding the peak (~550 to 900 K), with MLS typically up to 1.0 ppbv (~5-20%) lower, consistent with the results of *Santee et al.* [2007c, this issue]. Somewhat larger differences are seen in the mid to low EqL lower stratosphere, below ~500 K, and above ~900 K, with MLS biased low. ACE-FTS does not capture the region of lowest HNO_3 in the NH lower stratospheric vortex indicative of sequestration in PSCs, an effect of the sparse sampling of ACE missing the region of strongest PSC activity, which is not aligned with PV contours and is limited in spatial extent.

4.3.2. HCl As a primary chlorine reservoir species, HCl also plays an important role in polar processing in the lower stratosphere [e.g., *Solomon*, 1999]. EqL/time evolution of MLS v2.2 and ACE-FTS HCl in the lower stratosphere during the 2004-2005 NH winter (not shown) indicates very good quantitative agreement in the evolution of the region of low HCl associated with chlorine activation, and in other features of the time evolution. Figure 20 shows EqL/θ comparisons of MLS v2.2, ACE-FTS, and HALOE HCl in January 2005. Agreement between ACE-FTS and MLS is very good, typically better than 5%, everywhere above ~550 K, consistent with *Froidevaux et al.* [2007a, this issue]. In the low-HCl region in the NH vortex, ACE-FTS is higher than MLS by up to ~0.4 ppmv, resulting from ACE-FTS sampling not covering the location of minimum values in the vortex core sampled by MLS. HALOE HCl is ~5–25% lower than MLS through most of the range, consistent with *Froidevaux et al.* [2007a, this issue]. Because the depletion of the reservoir HCl by activation of Cl is largely well-

correlated with the vortex, sampling effects on HCl comparisons are minimal.

4.3.3. Temperature The use of vortex centered (i.e., EqL) coordinates is not an obvious choice for temperature from a scientific point of view, since temperature is not, in general, expected to be closely spatially correlated with the vortex [e.g., *Manney et al.*, 1996a, 2003b; *Mann et al.*, 2002]. However, we are often interested in temperatures within the vortex, and the comparison between MLS and solar occultation instruments can help us understand how the sparse sampling of the solar occultation instruments may affect studies of processes depending on temperature. Also, the EqL coordinate still provides a method of comparing solar occultation measurements with other datasets over a broader range of conditions than can easily be done with individual coincidences or zonal means.

Figure 21 compares EqL/θ-mapped MLS and ACE-FTS temperatures in September 2005, during the SH late winter. MLS appears lower than ACE-FTS almost everywhere, by a much larger amount than the small bias noted by *Schwartz et al.* [2007, this issue]. During this period, there was strong wave activity throughout the stratosphere, with the vortex distorted and shifted off the pole, and a dipole pattern of low/high temperatures across the vortex edge on the side with the anticyclone (Figure 22). ACE-FTS measurements were in the outer part of the vortex, so tended to miss the coldest region and sample near the warmest region on most days during the period (Figure 22), resulting in the apparent low bias of MLS with respect to ACE-FTS. This shows how strong a factor sampling is in comparisons of temperature, and demonstrates the care that must be taken in interpreting temperatures in vortex-centered coordinates.

5. Summary and Outlook

Derived meteorological products (DMPs) have been calculated and made available for Aura MLS and the solar occultation instruments ACE-FTS, MAESTRO, HALOE, POAM II and III, and SAGE II and III. The DMPs are fields calculated from gridded meteorological analyses that are interpolated to the observation locations of the satellite instruments. The DMP fields include θ, horizontal winds, PV, horizontal PV gradients, EqL, geopotential height, vortex edge criteria, and tropopause locations; DMP files for some instruments include additional potentially useful quantities such as temperature gradients and line-of-sight PV and temperature gradients. The DMPs have been calculated from the Met Office stratosphere-troposphere assimilation dataset for all instruments; in addition, DMPs from GEOS-4 and GEOS-5 are available for ACE-FTS and MLS, and from NCEP/CPC data for SAGE II. DMPs are not limited to the Aura mission, but have been calculated for the entire mission for each instrument. DMPs are provided (see Appendix) with the hope that other researchers will find them useful both for validation and in science studies combining multiple datasets.

Examples comparing MLS and solar occultation data were used to illustrate sampling issues. Situations in which sampling effects can be important include:

- Comparison of fine-scale transport features (e.g., filaments and intrusions into the vortex) as represented in high-resolution gridded meteorological analyses and in MLS data.
- Studies using "vortex averages" of long-lived tracers to estimate descent, where the movement of solar occultation sampling from vortex edge to vortex center over time can result in erroneous estimates of descent.
- Studies of O_3 in the middle stratosphere in low-O_3 pockets, where the combination of chemical and dynamical processes results in O_3 distributions that are not closely aligned with the vortex.
- Localized features (such as PSC-induced depressions in gas-phase HNO_3) that are captured by MLS but not by sparse solar occultation sampling.
- Comparisons during polar winter when the temperature field is typically not well-correlated with the vortex, such that sparse solar occultation sampling misses extreme values.

Solar occultation data are extremely valuable for understanding the atmosphere and monitoring its long-term changes, because of their high vertical resolution and precision, the availability of long, calibrated datasets (e.g., SAGE II, HALOE, POAM), and the potential for detecting many species (e.g., ACE-FTS). Even greater value is realized in studies combining solar occultation with other data, such as those from UARS MLS [e.g. *Manney et al.*, 1999, 2000; *Randel et al.*, 1999] and Aura MLS [*Braathen et al.*, 2006; *Singleton et al.*, 2007; *Santee et al.*, 2007b]. The spatial sparsity of the solar occultation data makes understanding sampling effects critical; sampling limitations have been studied here using DMPs to help guide interpretation of the solar occultation data and combination of them with other datasets.

Several of the examples shown here indicate good agreement in time evolution and spatial structure of MLS and solar occultation observations when mapped using DMPs, complementing traditional validation studies shown in other papers in this special issuer. For these types of studies, using

DMPs to combine MLS and solar occultation datasets in a consistent framework is a powerful analysis tool. Two such areas are transport studies based on long-lived tracers, and polar processing in the winter lower stratosphere.

Comparisons of MLS and ACE-FTS long-lived trace gas measurements show:

- ACE-FTS and MLS v2.2 CO and H_2O provide a similar picture of the descent of mesospheric air into the stratospheric vortex, both in magnitude and timing.
- MLS v2.2 N_2O and H_2O show excellent agreement with ACE-FTS data in EqL/time evolution in the middle and lower stratosphere
- MLS v2.2 and ACE-FTS CO show excellent agreement in EqL/time evolution in the middle and upper stratosphere.
- MLS v2.2 N_2O shows a persistent low bias with respect to ACE-FTS in the polar lower stratosphere. Elsewhere, differences are typically within $\sim$5 ppbv, with localized differences up to $\sim$15 ppbv.
- MLS v2.2 and ACE-FTS H_2O agree very well throughout the stratosphere, typically to within 5%. HALOE H_2O shows a persistent low bias with respect to MLS of $\sim$5–10%, consistent with previous studies.
- MLS v2.2 and ACE-FTS CO compare very well qualitatively, and overall quantitatively; however, MLS CO data are noisy and still characterized by some vertical oscillations in the stratosphere that compromise detailed quantitative agreement.

The effects of sampling differences on these comparisons are minimal, except for the "vortex-averages" described above. Using EqL-mapping of long-lived tracers thus facilitates combining solar occultation and MLS datasets for transport studies.

Good agreement is also seen in most analyses of species involved in lower stratospheric polar processing:

- Time evolution and values of O_3 in the lower stratospheric vortex agree well between MLS v2.2 and ACE-FTS, MAESTRO, POAM III, and SAGE III (the solar occultation instruments with good coverage of the vortex), and all instruments show a similar amount of decrease related to chemical O_3 loss.
- O_3 agrees to within 5% from tropopause level through the lower stratosphere, with larger differences only at higher levels where chemical processes that are not well-correlated with the vortex become important.
- MLS v2.2 and ACE-FTS HNO_3 agree very well qualitatively, but MLS shows a low bias with respect to ACE-FTS; agreement in morphology and time evolution in the lower stratosphere is good, except when ACE-FTS sampling misses regions of PSCs.
- MLS v2.2 and ACE-FTS HCl agree well throughout the stratosphere; HALOE HCl is $\sim$5–25% lower than MLS and ACE-FTS. Morphology and time evolution of MLS and ACE-FTS HCl in and around the lower stratospheric vortex agree well.

The good agreement and limited impact of sampling issues imply that vortex-centered analyses are useful for detailed polar-processing studies.

Further work to add to and improve DMPs is planned, including calculating DMPs for all solar occultation datasets from GEOS-4 (and, when the reanalysis is completed, GEOS-5) data, and calculating DMPs for SAGE I and possibly for other datasets, such as UARS MLS and UARS Cryogenic Limb Array Etalon Spectrometer. We hope to continue operational production of the DMPs for MLS and ACE-FTS for the duration of those missions. A procedure is available for users to request DMPs calculated at locations that they define (see Appendix); this system is being used to produce DMPs for ACE-FTS validation campaigns [e.g., *Walker et al.*, 2005; *Kerzenmacher et al.*, 2005] conducted in Eureka in 2004 through 2007 and planned for 2008. *Manney et al.* [2007] used Eureka DMP products along with ACE-FTS, MLS, Sounding of the Atmosphere through Broadband Emission Radiometry, and ground-based data to provide a meteorological context for the 2004, 2005 and 2006 campaigns, and they, and ACE DMPs, are being used in other ACE validation studies. We are using the DMPs in several studies combining solar occultation datasets and MLS data, and hope that they will be useful to other researchers in similar efforts.

Appendix: DMP Access, File Format, and Usage

Table 3 shows the locations for solar occultation DMP access via anonymous ftp from mls.jpl.nasa.gov; these can also be accessed from the MLS webpage (http://mls.jpl.nasa.gov) under http://mls.jpl.nasa.gov/research/meteorology.php. The ACE-FTS DMPs are provided to the ACE-FTS Science Team and distributed by them. For information on these products, please contact ACE-FTS Mission Scientist Peter Bernath (info@acebox.uwaterloo.ca).

DMPs can also be obtained by request at user-defined (UD) times/locations; see http://mls.jpl.nasa.gov/docs/genericDMPdescription.txt

Table 3. Availability of solar occultation Instrument DMPs via FTP

Mission/Instrument	Location[1]	Types	Time range
ACE	Distributed by ACE team	MetO, GEOS{4,5}	2004/01–present
SAGE II[2]	sage2/dmp/v5.0	NCEP/CPC	1984/10-2005/08
	sage2/dmp/v5.0	MetO	1991/10-2005/08
SAGE III[2]	sage3/v03.00/dmp/g3asmb/v1.1/<y>/<d>[3]	MetO	2002/05–2005/12
POAM II[2]	poam2/v6.00/dmp/v1.0	MetO	1993/10–1996/11
POAM III[2]	poam3/v4.00/dmp/v1.0	MetO	1998/04–2005/12
HALOE	haloe/v19/dmp/v1.1/<y>	MetO	1991/10–2005/11

[1]Relative to pub/outgoing/manney after logging in via FTP
[2]Example software for reading SAGE II and III and POAM II and III DMPs can be found at https://www.openchannelsoftware.com/projects/Example_IDL_Readers_for_DMPs
[3]<y>=4-digit year, <d>=3-digit day-of-year

for information on how to make such a request and the format for the input files.

Aura MLS DMPs are publicly available at http://mls.jpl.nasa.gov/dmp. Users must first request access and agree not to redistribute the MLS DMP files. This access request is not intended as a restriction, but rather as a means to gauge community uses for these products and to provide users with updates and information on changes or problems. MLS DMPs can be downloaded for v1.5 and v2.2, GEOS-4 or 5 and MetO, for the full Aura mission.

The formats of the DMP files are designed to follow as closely as possible the formats of the datasets they are provided for. Information on the file formats and links to sample read software are provided on the ftp or web sites along with the DMPs.

Acknowledgments. We thank the JPL MLS Science Team, especially Robert P. Thurstans, Ryan Fuller, Brian J. Mills, Paul A. Wagner, and Xuan Sabounchi, for their continuing support and assistance, Sharon Burton and Nina Iyer for assistance with SAGE II data, Randy Moore and David Risley for assistance with SAGE III data, and three anonymous reviewers for their helpful comments. Past and present members of the Met Office Assimilation Applications Group (formerly Middle Atmosphere Group) have been responsible for developing the MetO-SST dataset, and for maintaining the daily operational flow of these data; MetO data are provided by the British Atmospheric Data Centre. Research at the Jet Propulsion Laboratory, California Institute of Technology, is done under contract with the National Aeronautics and Space Administration. Funding for the ACE mission was provided primarily by the Canadian Space Agency and the Natural Sciences and Engineering Research Council of Canada.

References

Allen, D. R., J. L. Stanford, M. A. López-Valverde, N. Nakamura, D. J. Lary, A. R. Douglass, M. C. Cerniglia, J. J. Remedios, and F. W. Taylor (1999), Observations of middle atmosphere CO from the UARS ISAMS during the early northern winter 1991/1992, *J. Atmos. Sci.*, *56*, 563–583.

Barrett, B., et al. (2006), Intercomparisons of trace gas profiles from the Odin/SMR and Aura/MLS limb sounders, *J. Geophys. Res.*, *111*, D21,302, doi:10.1029/2006JD007,305, 2006.

Bernath, B. F., et al. (2005), Atmospheric Chemistry Experiment (ACE): mission overview, *Geophys. Res. Lett.*, *32*, L15S01, doi:10.1029/2005GL022,386.

Bethan, S., G. Vaughan, and S. J. Reid (1996), A comparison of ozone and thermal tropopause heights and the impact of tropopause definition on quantifying the ozone content of the troposphere, *Q. J. R. Meteorol. Soc.*, *122*, 929–944.

Birner, T., A. Dörnbrack, and U. Schumann (2002), How sharp is the tropopause at midlatitudes?, *Geophys. Res. Lett.*, *29*, 10.1029/2002GL015,142.

Bloom, S. C., L. L. Takacs, A. M. da Silva, and D. Ledvina (1996), Data assimilation using incremental analysis updates, *Mon. Weather Rev.*, *124*, 1256–1271.

Bloom, S. C., et al. (2005), The Goddard Earth Observing Data Assimilation System, GEOS DAS Version 4.0.3: Documentation and validation, *Tech. Rep. 104606 V26*, NASA.

Boone, C. D., R. Nassar, K. A. Walker, Y. Rochon, S. D. McLeod, C. P. Rinsland, and P. F. Bernath (2005), Retrievals for the Atmospheric Chemistry Experiment Fourier-Transform Spectrometer, *Appl. Opt.*, *44*, 7218–7231.

Borchi, F., and J.-P. Pommereau (2006), Evaluation of ozonesondes, HALOE, SAGE II and III, Odin-OSIRIS and SMR, and ENVISAT-GOMOS, -SCIAMACHY and -MIPAS ozone profiles in the tropics from SAOZ long duration balloon measurements in 2003 and 2004, *Atmos. Chem. Phys. Disc.*, *6*, 10,087–10,152.

Braathen, G., et al. (2006), Joint WMO/EU Arctic ozone bulletin, winter/spring summary, *Tech. Rep. 2006-1*, World Meteorological Organization/European Ozone Research Coordinating Unit, available at http://www.wmo.int/pages/prog/arep/gaw/ozone/index.html.

Butchart, N., and E. E. Remsberg (1986), The area of the stratospheric polar vortex as a diagnostic for tracer transport on an isentropic surface, *J. Atmos. Sci.*, *43*, 1319–1339.

Chiou, E., L. W. Thomason, S. P. Burton, and H. A. Michelsen (2004), Assessment of the SAGE II version

6.2 water vapor data set through intercomparison with ATMOS/ATLAS-3 measurments, *Geophys. Res. Lett.*, *31*, L14,101, doi:10.1029/2004GL020,071.

Chu, W. P., M. P. McCormick, J. Lenoble, C. Brogniez, and P. Pruvost (1989), SAGE II inversion algorithm, *J. Geophys. Res.*, *94*, 8339–8351.

Cunnold, D. M., W. P. Chu, R. A. Barnes, M. P. McCormick, and R. E. Veiga (1989), Validation of SAGE II ozone measurements, *J. Geophys. Res.*, *94*, 8447–8460.

Davies, T., M. J. P. Cullen, A. J. Malcolm, M. H. Mawson, A. Staniforth, A. A. White, and N. Wood (2005), A new dynamical core for the met office's global and regional modelling of the atmosphere, *Q. J. R. Meteorol. Soc.*, *131*, 1759–1782.

Derber, J. C., and W. Wu (1998), The use of TOVS cloud-cleared radiances in the NCEP SSI analysis system, *Mon. Weather Rev.*, *126*, 2287–2299.

Dufour, G., et al. (2005), Partitioning between the inorganic chlorine reservoirs HCl and $ClONO_2$ during the Arctic winter 2005 derived from the ACE-FTS measurements, *Atmos. Chem. Phys.*, *6*, 2355–2366.

Dunkerton, T. J., and D. P. Delisi (1986), Evolution of potential vorticity in the winter stratosphere of January-February 1979, *J. Geophys. Res.*, *91*, 1199–1208.

Finger, F. G., H. M. Woolf, and C. E. Anderson (1965), A method for objective analysis of stratospheric constant pressure charts, *Mon. Weather Rev.*, *93*, 619–638.

Finger, F. G., M. E. Gelman, J. D. Wild, M. L. Chanin, A. Hauchecorne, and A. J. Miller (1993), Evaluation of NMC upper-stratospheric temperature analyses using rocketsonde and lidar data, *Bull. Am. Meteorol. Soc.*, *74*, 789–799.

Froidevaux, L., et al. (2006), Early validation analyses of atmospheric profiles from EOS MLS on the Aura satellite, *IEEE Trans. Geosci. Remote Sens.*, *44*, 1106–1121.

Froidevaux, L., et al. (2007a), Validation of EOS MLS HCl measurements, *J. Geophys. Res.*, submitted, 2007. Available at http://mls.jpl.nasa.gov.

Froidevaux, L., et al. (2007b), Validation of EOS MLS stratospheric ozone measurements, *J. Geophys. Res.*, submitted, 2007. Available at http://mls.jpl.nasa.gov.

Fussen, D., F. Vanhellemont, J. Dodion, C. Bingen, K. A. Walker, C. D. Boone, S. D. McLeod, and P. F. Bernath (2005), Initial intercomparison of ozone and nitrogen dioxide number density profiles retrieved by the ACE-FTS and GOMOS occultation experiments, *Geophys. Res. Lett.*, *32*, L16S02, doi:10.1029/2005GL022,468.

Gelman, M. E., A. J. Miller, K. W. Johnson, and R. M. Nagatani (1986), Detection of long term trends in global stratospheric temperature from NMC analyses derived from NOAA satellite data, *Adv. Space. Res.*, *6(10)*, 17–26.

Gelman, M. E., A. J. Miller, R. M. Nagatani, and C. S. Long (1994), Use of UARS data in the NOAA stratospheric monitoring program, *Adv. Space. Res.*, *14(9)*, 21–31.

Glaccum, W., , et al. (1996), The Polar Ozone and Aerosol Measurement instrument, *J. Geophys. Res.*, *101*, 14,479–14,487.

Harvey, V. L., R. B. Pierce, M. H. Hitchman, C. E. Randall, and T. D. A. Fairlie (2004), On the distribution of ozone in stratospheric anticyclones, *J. Geophys. Res.*, *109*, D24308, doi:10.1029/2004JD004992.

Harvey, V. L., C. E. Randall, C. Singleton, and G. L. Manney (2007), Low-ozone pockets observed by EOS-MLS, *J. Geophys. Res.*, submitted, 2007. Available at http://mls.jpl.nasa.gov.

Highwood, E. J., and P. Berrisford (2000), Properties of the Arctic tropopause, *Q. J. R. Meteorol. Soc.*, *126*, 1515–1532.

Jiang, Y., et al. (2007), Aura Microwave Limb Sounder validation by ozonesonde and lidar measurements, *J. Geophys. Res.*, submitted, 2007. Available at http://mls.jpl.nasa.gov.

Jin, J. J., et al. (2006a), Denitrification in the Arctic winter 2004/2005: Observations from ACE-FTS, *Geophys. Res. Lett.*, *33*, L19,814, doi:10.1029/2006GL027,687.

Jin, J. J., et al. (2006b), Severe Arctic ozone loss in the winter 2004/2005: Observations from ACE-FTS, *Geophys. Res. Lett.*, *33*, L15,801, doi:10.1029/2006GL026,752.

Kar, J., et al. (2007), Initial comparison of ozone and NO_2 profiles from ACE-MAESTRO with balloon and satellite data, *J. Geophys. Res.*, in press, 2007.

Kerzenmacher, T. E., et al. (2005), Measurements of O_3, NO_2 and temperature during the 2004 Canadian Arctic ACE validation campaign, *Geophys. Res. Lett.*, *32*, L16S07, doi:10.1029/2005GL023,032.

Kley, D., et al. (2000), SPARC assessment of upper tropospheric and stratospheric water vapour, *Tech. Rep. SPARC Report No. 2*, WCRP-No. 113, WMO/TD-No, 104.

Lait, L. R., et al. (1990), Reconstruction of O_3 and N_2O fields from ER-2, DC-8, and balloon observations, *Geophys. Res. Lett.*, *17*, 521–524.

Lambert, A., et al. (2007), Validation of the Aura Microwave Limb Sounder stratospheric water vapor and nitrous oxide measurements, *J. Geophys. Res.*, in press, 2007. Available at http://mls.jpl.nasa.gov.

Livesey, N. J., et al. (2007a), Validation of Aura Microwave Limb Sounder O_3 and CO observations in the upper troposphere and lower stratosphere, *J. Geophys. Res.*, submitted, 2007. Available at http://mls.jpl.nasa.gov.

Livesey, N. J., et al. (2007b), MLS Version 2.2 level 2 data quality and description document, *Tech. Rep. JPL D-33509*, Jet Propulsion Laboratory, available at http://mls.jpl.nasa.gov.

Lorenc, A. C., R. S. Bell, and B. Macpherson (1991), The Meteorological Office analysis correction data assimilation scheme, *Q. J. R. Meteorol. Soc.*, *117*, 59–89.

Lorenc, A. C., et al. (2000), The Met. Office global three-dimensional variational data assimilation scheme, *Q. J. R. Meteorol. Soc.*, *126*, 2991–3012.

Lucke, R. L., et al. (1999), The Polar Ozone and Aerosol Measurement (POAM) III instrument and early validation results, *J. Geophys. Res.*, *104*, 18,785–18,799.

Lumpe, J. D., et al. (2002), POAM III retrieval algorithm and error analysis, *J. Geophys. Res.*, *107*, doi:10.1029/2002JD002,137.

Lumpe, J. D., et al. (2003), Comparison of POAM III ozone measurments with correlative aircraft and balloon data during SOLVE, *J. Geophys. Res.*, *108*, 8316, doi:10.1029/2001JD000,472.

Lumpe, J. D., et al. (2006), Validation of Polar Ozone and Aerosol Measurement (POAM) III version 4 stratospheric water vapor, *J. Geophys. Res.*, *111*, D11,301, doi:10.1029/2005JD006,763.

Mann, G. W., S. Davies, K. S. Carslaw, M. P. Chipperfield, and J. Kettleborough (2002), Polar vortex concentricity as a controlling factor in Arctic denitrification, *J. Geophys. Res.*, *107*, 4663 doi:10.1029/2002JD002,102.

Manney, G. L., R. W. Zurek, M. E. Gelman, A. J. Miller, and R. Nagatani (1994a), The anomalous Arctic lower stratospheric polar vortex of 1992–1993, *Geophys. Res. Lett.*, *21*, 2405–2408.

Manney, G. L., R. W. Zurek, A. O'Neill, and R. Swinbank (1994b), On the motion of air through the stratospheric polar vortex, *J. Atmos. Sci.*, *51*, 2973–2994.

Manney, G. L., L. Froidevaux, J. W. Waters, and R. W. Zurek (1995a), Evolution of Microwave Limb Sounder ozone and the polar vortex during winter, *J. Geophys. Res.*, *100*, 2953–2972.

Manney, G. L., M. L. Santee, L. Froidevaux, J. W. Waters, and R. W. Zurek (1996a), Polar vortex conditions during the 1995–96 Arctic winter: Meteorology and MLS ozone, *Geophys. Res. Lett.*, *23*, 3203–3206.

Manney, G. L., R. Swinbank, S. T. Massie, M. E. Gelman, A. J. Miller, R. Nagatani, A. O'Neill, and R. W. Zurek (1996b), Comparison of U. K. Meteorological Office and U. S. National Meteorological Center stratospheric analyses during northern and southern winter, *J. Geophys. Res.*, *101*, 10,311–10,334.

Manney, G. L., H. A. Michelsen, M. L. Santee, M. R. Gunson, F. W. Irion, A. E. Roche, and N. J. Livesey (1999), Polar vortex dynamics during spring and fall diagnosed using trace gas observations from the Atmospheric Trace Molecule Spectroscopy instrument, *J. Geophys. Res.*, *104*, 18,841–18,866.

Manney, G. L., H. A. Michelsen, F. W. Irion, M. R. Gunson, G. C. Toon, and A. E. Roche (2000), Lamination and polar vortex development in fall from ATMOS long-lived trace gases observed during November 1994, *J. Geophys. Res.*, *105*, 29,023–29,038.

Manney, G. L., W. A. Lahoz, J. L. Sabutis, A. O'Neill, and L. Steenman-Clark (2002), Simulations of fall and early winter in the stratosphere, *Q. J. R. Meteorol. Soc.*, *128*, 2205–2237.

Manney, G. L., L. Froidevaux, M. L. Santee, N. J. Livesey, J. L. Sabutis, and J. W. Waters (2003a), Variability of ozone loss during Arctic winter (1991 to 2000) estimated from UARS Microwave Limb Sounder measurements, *J. Geophys. Res.*, *108*, 4149, doi:10.1029/2002JD002,634.

Manney, G. L., J. L. Sabutis, S. Pawson, M. L. Santee, B. Naujokat, R. Swinbank, M. E. Gelman, and W. Ebisuzaki (2003b), Lower stratospheric temperature differences between meteorological analyses in two cold Arctic winters and their impact on polar processing studies, *J. Geophys. Res.*, *108*, 8328, doi:10.1029/2001JD001,149.

Manney, G. L., M. L. Santee, N. J. Livesey, L. Froidevaux, W. G. Read, H. C. Pumphrey, J. W. Waters, and S. Pawson (2005a), EOS Microwave Limb Sounder observations of the Antarctic polar vortex breakup in 2004, *Geophys. Res. Lett.*, *32*, L12,811, doi:10.1029/2005GL022,823.

Manney, G. L., M. L. Santee, L. Froidevaux, K. Hoppel, N. J. Livesey, and J. W. Waters (2006), EOS MLS observations of ozone loss in the 2004-2005 Arctic winter, *Geophys. Res. Lett.*, *33*, L04,802, doi:10.1029/2005GL024,494.

Manney, G. L., et al. (1995b), Formation of low-ozone pockets in the middle stratospheric anticyclone during winter, *J. Geophys. Res.*, *100*, 13,939–13,950.

Manney, G. L., et al. (2001), Comparison of satellite ozone observations in coincident air masses in early November 1994, *J. Geophys. Res.*, *106*, 9923–9944.

Manney, G. L., et al. (2005b), Diagnostic comparison of meteorological analyses during the 2002 Antarctic winter, *Mon. Weather Rev.*, *133*, 1261–1278.

Manney, G. L., et al. (2007), The high Arctic in extreme winters: Vortex, temperature, and MLS trace gas evolution, *Atmos. Chem. Phys. Disc.*, *7*, 10,235–10,285.

Mauldin, L. E., N. H. Zaun, M. P. McCormick, J. H. Guy, and W. R. Vaugh (1985), Stratospheric Aerosol and Gas Experiment II instrument: A functional description, *Opt. Eng.*, *24*, 307–312.

McCormick, M. P., J. M. Zawodny, R. E. Veiga, J. C. Larsen, and P. H. Wang (1989), An overview of SAGE I and SAGE II ozone measurements, *Planet. Space Sci.*, *37*, 1567–1586.

McCormick, M. P., et al. (2002), SAGE III algorithm theoretical basis document: Solar and lunar algorithm, *Tech. Rep. 475-00-108, Version 2.1*, NASA Langley Research Center.

McElroy, C. T., et al. (2007), The ACE-MAESTRO instrument on SCISAT: description, performance, and preliminary results, *Appl. Opt.*, *46*, 4341–4356.

McNally, A. P., J. C. Derber, W. Wu, and B. B. Katz (2000), The use of TOVS level-1b radiances in the NCEP SSI analysis system, *Q. J. R. Meteorol. Soc.*, *126*, 689–724.

Michelsen, H. A., et al. (2002), ATMOS version 3 water vapor measurements: Comparisons with ATMOS version 2 retrievals and observations from two ER-2 Lyman-α hygrometers, MkIV, MAS, HALOE, and MLS, *J. Geophys. Res.*, *107*, 10.1029/2001JD000,587.

Morris, G. A., S. R. Kawa, A. R. Douglass, M. R. Schoeberl, L. Froidevaux, and J. W. Waters (1998), Low-ozone pockets explained, *J. Geophys. Res.*, *103*, 3599–3610.

Morris, G. A., J. F. Gleason, J. M. R. III, M. R. Shoeberl, and M. P. McCormick (2002), A comparison of HALOE V19 with SAGE II V6.00 ozone observations using trajectory mapping, *J. Geophys. Res.*, *107*, 10.1029/2001JD000,847.

Nair, H., M. Allen, L. Froidevaux, and R. W. Zurek (1998), Localized rapid ozone loss in the northern winter stratosphere: An analysis of UARS observations, *J. Geophys. Res.*, *103*, 1555–1571.

Nash, E. R., P. A. Newman, J. E. Rosenfield, and M. R. Schoeberl (1996), An objective determination of the polar vortex using Ertel's potential vorticity, *J. Geophys. Res.*, *101*, 9471–9478.

Nassar, R., P. F. Bernath, C. D. Boone, G. L. Manney, S. D. McLeod, C. P. Rinsland, R. Skelton, and K. A. Walker (2005), Stratospheric abundances of water and methane based on ACE-FTS measurements, *Geophys. Res. Lett.*, *32*, L15S04, doi:10.1029/2005GL022,383.

Newman, P. A., L. R. Lait, M. R. Schoeberl, R. M. Nagatani, and A. J. Krueger (1989), Meteorological atlas of the Northern Hemisphere lower stratosphere for January and February 1989 during the Airborne Arctic Stratospheric Expedition, *Tech. Rep. 4145*, NASA.

Orsolini, Y. J., G. L. Manney, M. L. Santee, and C. E. Randall (2005a), An upper stratospheric layer of enhanced HNO_3 following exceptional solar storms, *Geophys. Res. Lett.*, *32*, L12,801, doi:10.1029/2004GL021,588.

Orsolini, Y. J., C. E. Randall, G. L. Manney, and D. R. Allen (2005b), An observational study of the final breakdown of the southern hemisphere stratospheric vortex in 2002, *J. Atmos. Sci.*, *62*, 735–747.

Pan, L., S. Solomon, W. Randel, J. F. Lamarque, P. Hess, J. Gille, E. W. Chiou, and M. P. McCormick (1997), Hemispheric asymmetries and seasonal variations of the lowermost stratospheric water vapor and ozone deprived from SAGE II data, *J. Geophys. Res.*, *102*, 28,117–28,184.

Petelina, S. V., et al. (2005), Validation of ACE-FTS stratospheric ozone profiles against Odin/OSIRIS measurements, *Geophys. Res. Lett.*, *32*, L15S06, doi:10.1029/2005GL022,377.

Pumphrey, H. C., et al. (2007), Validation of the Aura Microwave Limb Sounder stratospheric and mesospheric CO measurements, *J. Geophys. Res.*, in press, 2007. Available at http://mls.jpl.nasa.gov.

Randall, C. E., et al. (2002), Validation of POAM III NO_2 measurements, *J. Geophys. Res.*, *107*, 4432, doi:10.1029/2001JD001,520.

Randall, C. E., et al. (2003), Validation of POAM III ozone: Comparisons with ozonesonde and satellite data, *J. Geophys. Res.*, *108*, 4367, doi:10.1029/2002JD002,944.

Randall, C. E., et al. (2005), Stratospheric effects of energetic particle precipitation in 2003-2004, *Geophys. Res. Lett.*, *32*, L05,802, doi:10.1029/2004GL022,003.

Randel, W. J. (1987), The evaluation of winds from geopotential height data in the stratosphere, *J. Atmos. Sci.*, *44*, 3097–3120.

Randel, W. J., F. Wu, J. M. Russell, III, and J. W. Waters (1999), Space-time patterns of trends in stratospheric constituents derived from UARS measurements, *J. Geophys. Res.*, *104*, 3711–3727.

Redaelli, G., et al. (1994), UARS MLS O_3 soundings compared with lidar measurements using the conservative coordinates reconstruction technique, *Geophys. Res. Lett.*, *21*, 1535–1538.

Reichler, T., M. Dameris, and R. Sausen (2003), Determining the tropopause height from gridded data, *Geophys. Res. Lett.*, *30*, 2042, doi:10.1029/2003GL018,240.

Reinecker, M. M., et al. (2007), The GEOS-5 data assimilation system: A documentation of GEOS-5.0, *Tech. Rep. 104606 V27*, NASA.

Remsberg, E. E., et al. (2002), An assessment of the quality of HALOE temperature profiles in the mesosphere based on comparisons with Rayleigh backscatter lidar and inflatable falling sphere measurements, *J. Geophys. Res.*, *107*, doi:10.1029/2001JD001,521.

Rinsland, C. P., C. Boone, R. Nassar, K. Walker, P. Bernath, J. C. McConnell, and L. Chiou (2005), Atmospheric Chemistry Experiment (ACE) Arctic stratospheric measurements of NO_x during February and March 2004: Impact of intense solar flares, *Geophys. Res. Lett.*, *32*, L16S05, doi:10.1029/2005GL022,425.

Russell, J. M., III, et al. (1993), The Halogen Occultation Experiment, *J. Geophys. Res.*, *98*, 10,777–10,797.

Santee, M. L., G. L. Manney, N. J. Livesey, and W. G. Read (2004), Three-dimensional structure and evolution of stratospheric HNO_3 based on UARS Microwave Limb Sounder measurements, *J. Geophys. Res.*, *109*, D15,306, doi:10.1029/2004JD004,578.

Santee, M. L., et al. (2007a), Validation of the Aura Microwave Limb Sounder ClO measurements, *J. Geophys. Res.*, submitted, 2007. Available at http://mls.jpl.nasa.gov.

Santee, M. L., et al. (2007b), A study of stratospheric chlorine partitioning based on new satellite measurements and modeling, *J. Geophys. Res.*, submitted, 2007. Available at http://mls.jpl.nasa.gov.

Santee, M. L., et al. (2007c), Validation of the Aura Microwave Limb Sounder HNO_3 measurements, *J. Geophys. Res.*, submitted, 2007. Available at http://mls.jpl.nasa.gov.

Schoeberl, M. R. (2004), Extratropical stratosphere-troposphere mass exchange, *J. Geophys. Res.*, *109*, D13,303, doi:10.1029/2004JD004,525.

Schoeberl, M. R., M. Luo, and J. E. Rosenfield (1995), An analysis of the Antarctic Halogen Occultation Experiment trace gas observations, *J. Geophys. Res.*, *100*, 5159–5172.

Schoeberl, M. R., et al. (2006), Chemical observations of a polar vortex intrusion, *J. Geophys. Res.*, *111*, D20,306, doi:10.1029/2006JD007,134.

Schwartz, M. J., et al. (2007), Validation of the Aura Microwave Limb Sounder temperature and geopotential height measurements, *J. Geophys. Res.*, submitted, 2007. Available at http://mls.jpl.nasa.gov.

Sica, R. J., et al. (2007), Validation of ACE temperature using ground-based and space-based meassurements, *Atmos. Chem. Phys.*, submitted, 2007. Available at http://mls.jpl.nasa.gov.

Singleton, C. S., et al. (2007), Quantifying Arctic ozone loss during the 2004-2005 winter using satellite observations and a chemical transport model, *J. Geophys. Res.*, in press, 2007.

Solomon, S. (1999), Stratospheric ozone depletion: A review of concepts and history, *Rev. Geophys.*, *37*, 275–316.

Solomon, S., R. R. Garcia, J. J. Olivero, R. M. Bevilacqua, P. R. Schwartz, R. T. Clancy, and D. O. Muhleman (1985), Photochemistry and transport of carbon monoxide in the middle atmosphere, *J. Atmos. Sci.*, *42*, 1072–1083.

Stajner, I., C. Benson, H. C. Liu, S. Pawson, N. Brubaker, L.-P. Chang, L. P. Riishojgaard, and R. Todling (2007), Ice polar stratospheric clouds detected from assimilation of atmospheric infrared sounder data, *Geophys. Res. Lett.*, in press, 2007.

Swinbank, R., and A. O'Neill (1994), A stratosphere-troposphere data assimilation system, *Mon. Weather Rev.*, *122*, 686–702.

Swinbank, R., N. B. Ingleby, P. M. Boorman, and R. J. Renshaw (2002), A 3D variational data assimilation system for the stratosphere and troposphere, *Tech. Rep. 71*, Met Office Numerical Weather Prediction Forecasting Research Scientific Paper.

Swinbank, R., M. Keil, D. R. Jackson, and A. A. Scaife (2004), Stratospheric data assimilation at the Met Office - progress and plans, in *ECMWF workshop on Modelling and Assimilation for the Stratosphere and Tropopause 23-26-June, 2003*, ECMWF.

Taha, G., L. W. Thomason, and S. P. Burton (2004), Comparison of stratospheric aerosol and gas experiment (SAGE) II version 6.2 water vapor with balloon-borne and space-based instruments, *J. Geophys. Res.*, *109*, D18,313, doi:10.1029/2004JD004,859.

Thomason, L. W., L. R. Poole, and C. E. Randall (2006), SAGE III aerosol extinction validation in the Arctic winter: comparisons with SAGE II and POAM III, *Atmos. Chem. Phys. Disc.*, *2006, No. 6*, 11,357–11,389.

Walker, K. A., C. E. Randall, C. R. Trepte, C. D. Boone, and P. F. Bernath (2005), Initial validation comparisons for the Atmospheric Chemistry Experiment (ACE), *Geophys. Res. Lett.*, *32*, L16S04, doi:10.1029/2005GL022,388.

Wang, H.-J., D. M. Cunnold, L. W. Thomason, J. M. Zawodny, and G. E. Bodeker (2002), Assessment of SAGE version 6.1 ozone data quality, *J. Geophys. Res.*, *107*, 4691, doi:10.1029/2002JD002,418.

Wang, H.-J., D. M. Cunnold, C. Trepte, L. W. Thomason, and J. M. Zawodny (2006a), SAGE III solar ozone measurements: Initial results, *Geophys. Res. Lett.*, *33*, L03,805, doi:10.1029/2005GL025,099.

Wang, P.-H., D. M. Cunnold, C. Trepte, H. J. Wang, P. Jing, J. Fishman, V. G. Brackett, J. M. Zawodny, and G. E. Bodeker (2006b), Ozone variability in the midlatitude upper troposphere and lower stratosphere diagnosed from a monthly SAGE II climatology relative to the tropopause, *J. Geophys. Res.*, *111*, D21,304, doi:10.1029/2005JD006,108.

Waters, J. W., et al. (2006), The Earth Observing System Microwave Limb Sounder (EOS MLS) on the Aura satellite, *IEEE Trans. Geosci. Remote Sens.*, *44*, 1075–1092.

WMO (2007), Scientific assessment of stratospheric ozone depletion: 2006, U. N. Environ. Program, Geneva, Switzerland.

Wu, W.-S., R. J. Purser, and D. F. Parish (2002), Three-dimensional variational analyses with spatially inhomogeneous covariances, *Mon. Weather Rev.*, *130*, 2905–2916.

Gloria L. Manney, Mail Stop 183-701. Jet Propulsion Laboratory, California Institute of Technology, Pasadena, CA 91109, USA, Gloria.L.Manney@jpl.nasa.gov

This preprint was prepared with AGU's LaTeX macros v5.01, with the extension package 'AGU^{++}' by P. W. Daly, version 1.6b from 1999/08/19.

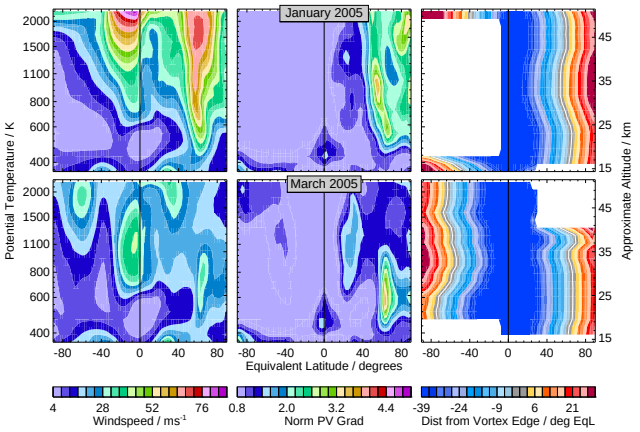

Figure 1. Monthly averages of equivalent latitude (EqL)/potential temperature (θ)-mapped (left to right) windspeed (ms^{-1}), normalized (see text) horizontal PV gradient, and distance in EqL from the vortex edge center (°EqL, see text). EqL/θ mapping is from derived meteorological products (DMPs) calculated from GEOS-4 data for MLS locations, during (top) January 2005 and (bottom) March 2005. White space in EqL from vortex edge plots indicates that the vortex is not defined anytime during the month in these regions.

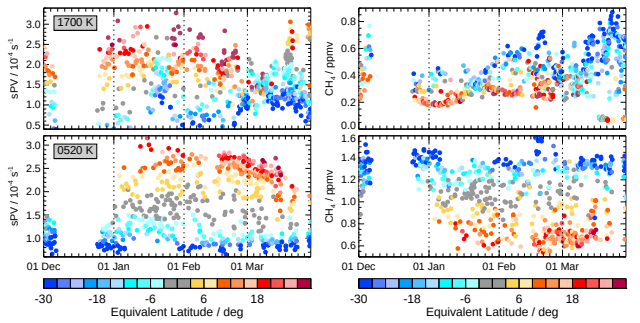

Figure 2. Timeseries of distance in EqL from vortex edge center (colors, °EqL) as a function of (left) sPV (10^{-4} s^{-1}) and (right) ACE-FTS CH_4 (ppmv) at (top) 1700 K and (bottom) 520 K, for ACE measurement locations during December 2004 through March 2005. Vortex edge location values are from GEOS-4 DMPs.

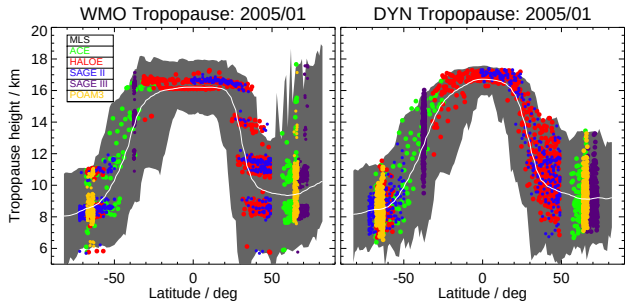

Figure 3. (Left) WMO and (right) dynamical (see text) tropopause altitudes from MetO DMPs for MLS (range shown as grey shading, white line average), ACE (green), HALOE (red), SAGE II (blue), SAGE III (purple) and POAM III (gold) for all measurements in January 2005. Tropopause pressures from MLS DMPs are converted to altitude using a scale height of 7.0 km.

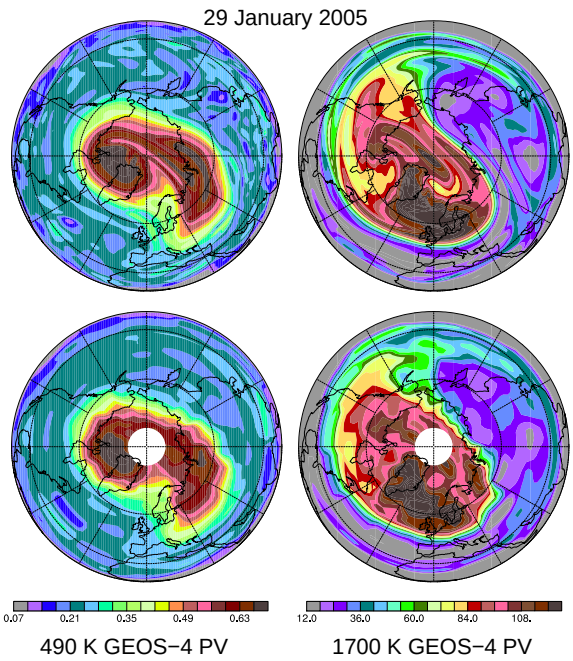

Figure 4. PV (10^{-4} K m^2 kg^{-1} s^{-1}) maps from GEOS-4 analyses (top row) and gridded (see text) from the MLS GEOS-4 DMP PV field (bottom row), at 490 K (left) and 1700 K (right). Projection is orthographic, with 0° longitude at the bottom and 90°E to the right; latitude range is from 0° to 90°N; fine dashed lines show a 30° latitude/longitude grid. White space above ∼82°N in lower panels is region not sampled by MLS.

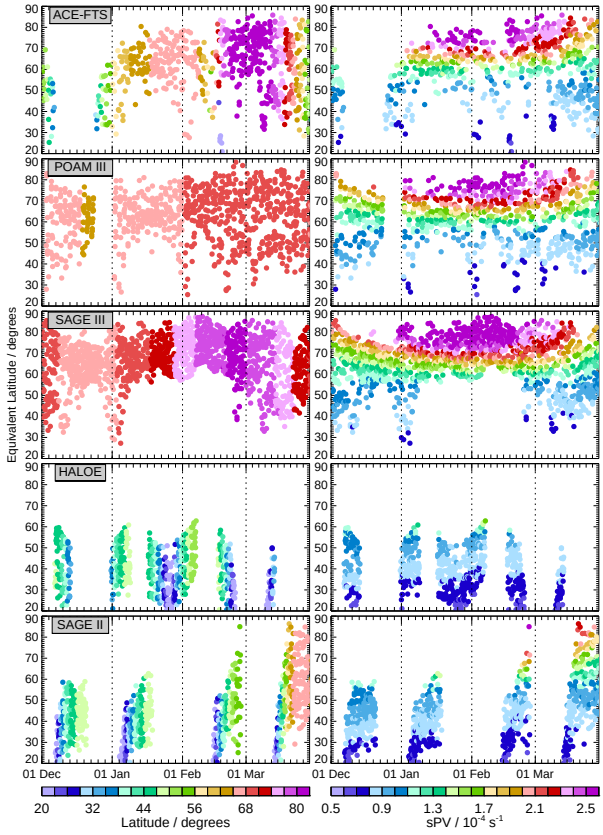

Figure 5. EqL/time plots of latitude (°, left) and sPV (10^{-4} s^{-1}) sampled by (top to bottom) ACE, POAM III, SAGE III, HALOE, and SAGE II during December 2004 through March 2005 EqL on the 490 K isentropic surface.

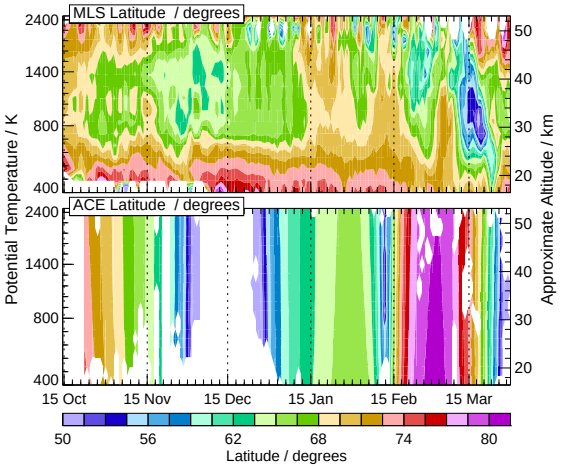

Figure 6. Vortex-averaged (within the 1.4 $\times 10^{-4}$ s^{-1} sPV contour, see text, from GEOS-4 DMPs) latitude (°) sampled by (top) MLS and (bottom) ACE from 15 October 2004 through 31 March 2005.

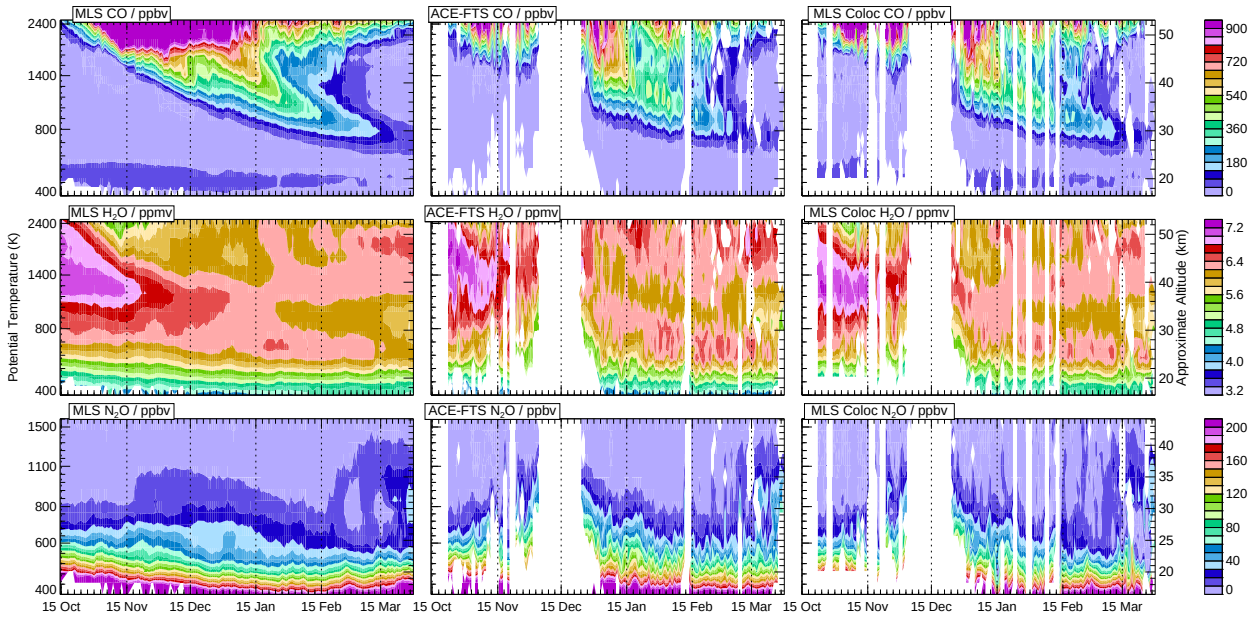

Figure 7. Vortex-averages (within 1.4×10^{-4} s^{-1} sPV contour, see text, from GEOS-4 DMPs) for 3 October 2004 through 31 March 2005 of (top to bottom) CO (ppbv), H_2O (ppmv), and N_2O (ppbv) from (left) MLS v1.5, (center) ACE-FTS, and (right) MLS v1.5 measurements coincident with ACE (see text). Vertical range is 400 to 2500 K for CO and H_2O, 400 to 1600 K for N_2O.

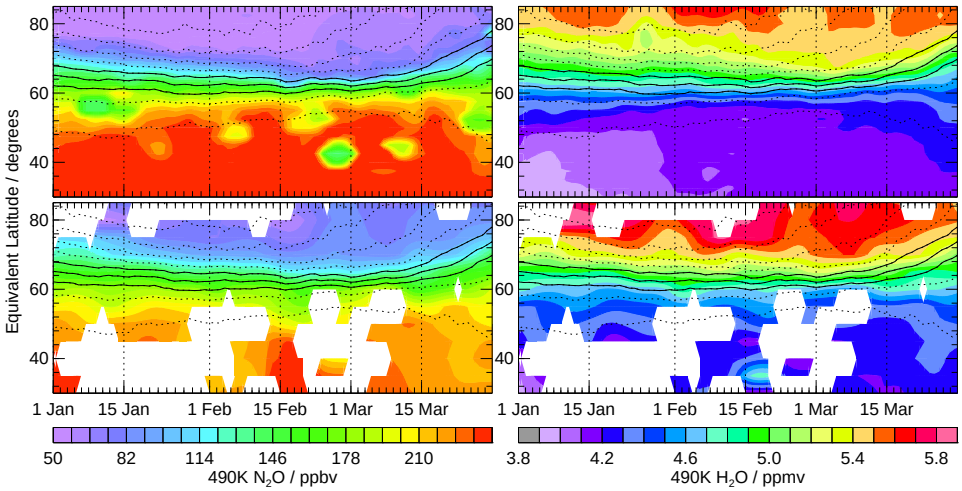

Figure 8. EqL/time series for 1 January through 31 March 2005 of MLS v2.2 (top) and ACE-FTS (bottom) N_2O (ppbv, left) and H_2O (ppmv, right) at 490 K, using GEOS-4 DMPs.

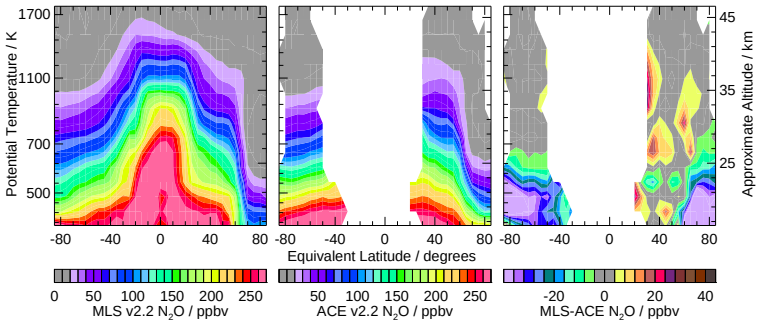

Figure 9. Global EqL/θ cross-sections for 10–16 March 2005 comparing MLS v2.2 with ACE-FTS N_2O. Left panel shows MLS v2.2 N_2O, center panel, ACE-FTS N_2O, and right panel the MLS−ACE-FTS N_2O difference (ppbv). GEOS-5 DMPs are used for EqL/θ mapping. Vertical range is 400 through 1800 K.

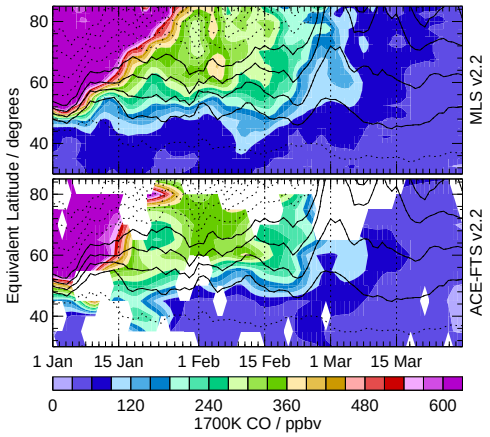

Figure 11. As in Figure 13, but for MLS v2.2 (top) and ACE-FTS (bottom) CO (ppbv) at 1700 K, using GEOS-4 DMPs.

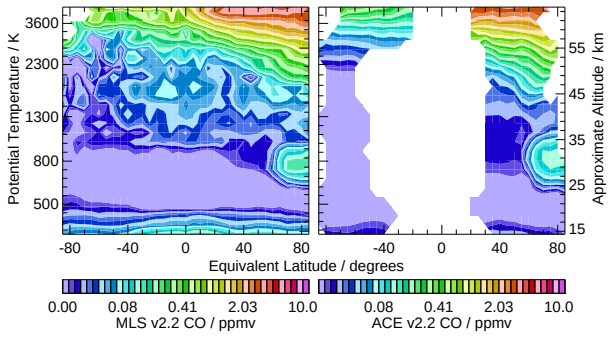

Figure 12. As in Figure 9 (with difference panel omitted), but for MLS v2.2 CO (ppbv) compared with ACE-FTS, using GEOS-5 DMPs. Vertical range is 360–4300 K. CO contour interval is on a log scale, from 20 to 10,000 ppbv.

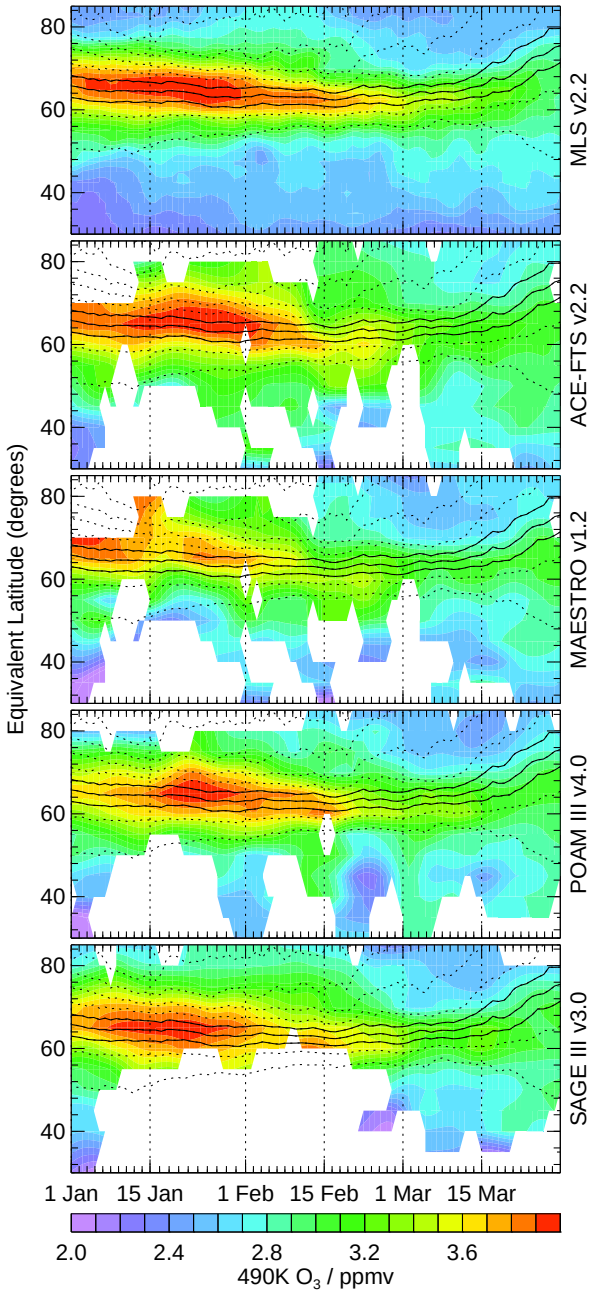

Figure 13. EqL/time series for 1 January through 31 March 2005 of O_3 (ppmv) at 490 K from (top to bottom) MLS (v2.2), ACE-FTS, MAESTRO, POAM III, and SAGE III. EqL mapping is done with MetO DMPs. Overlaid contours are MetO sPV (10^{-4} s^{-1}), with three contours in the vortex edge region shown as solid lines.

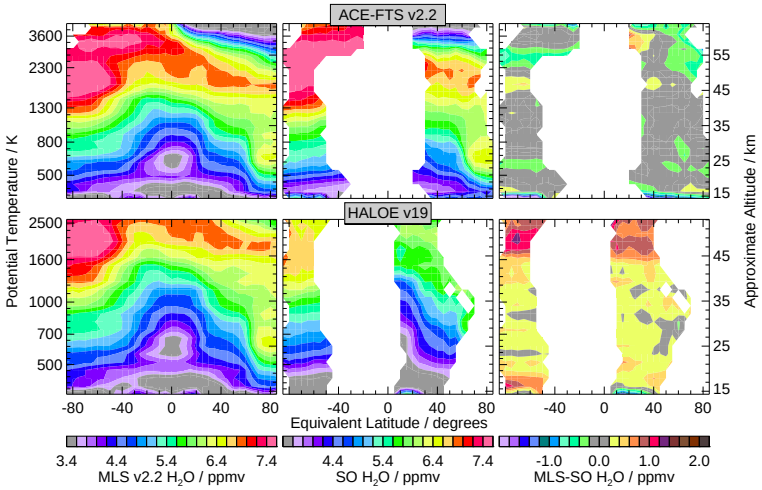

Figure 10. As in Figure 9, but for MLS v2.2 H_2O (ppmv) compared with (top) ACE-FTS and (bottom) HALOE. GEOS-5 DMPs are used for ACE-FTS comparison and MetO for HALOE comparison. Vertical range for ACE-FTS comparison is 360–4300 K, for HALOE comparison, 360–2500 K.

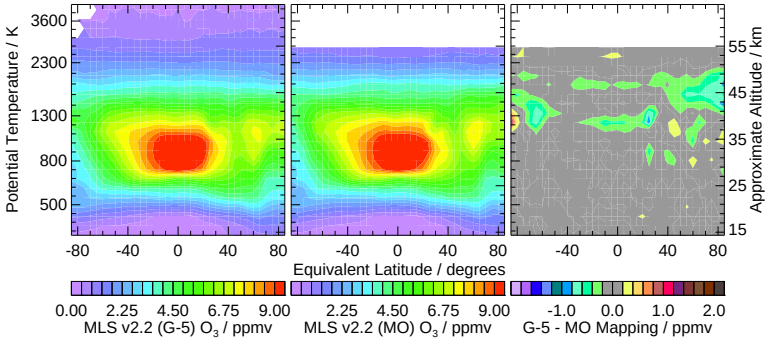

Figure 15. Global EqL/θ cross-sections for 10–16 March 2005 comparing MLS v2.2 O_3 (ppmv) mapped using GEOS-5 (left) and MetO (center) DMPs, and the difference (ppmv, right). Vertical range is 360 through 4300 K.

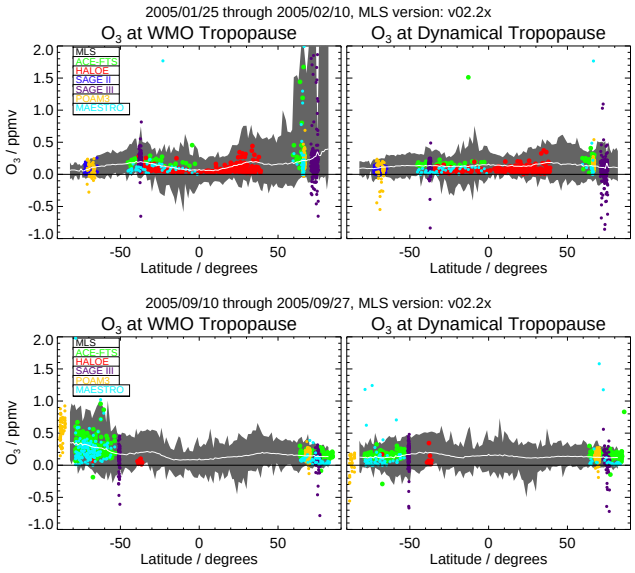

Figure 14. O_3 (ppmv) at the (left) WMO and (right) dynamical tropopause for MLS v2.2 (range shown as grey shading, average white line), ACE-FTS (green), MAESTRO (cyan), HALOE (red), SAGE II (blue), SAGE III (purple) and POAM III (gold) for all measurements during (top) 24 January–10 February 2005 and (bottom) 10–27 September 2005. Tropopause locations for interpolation of O_3 are from MetO DMPs.

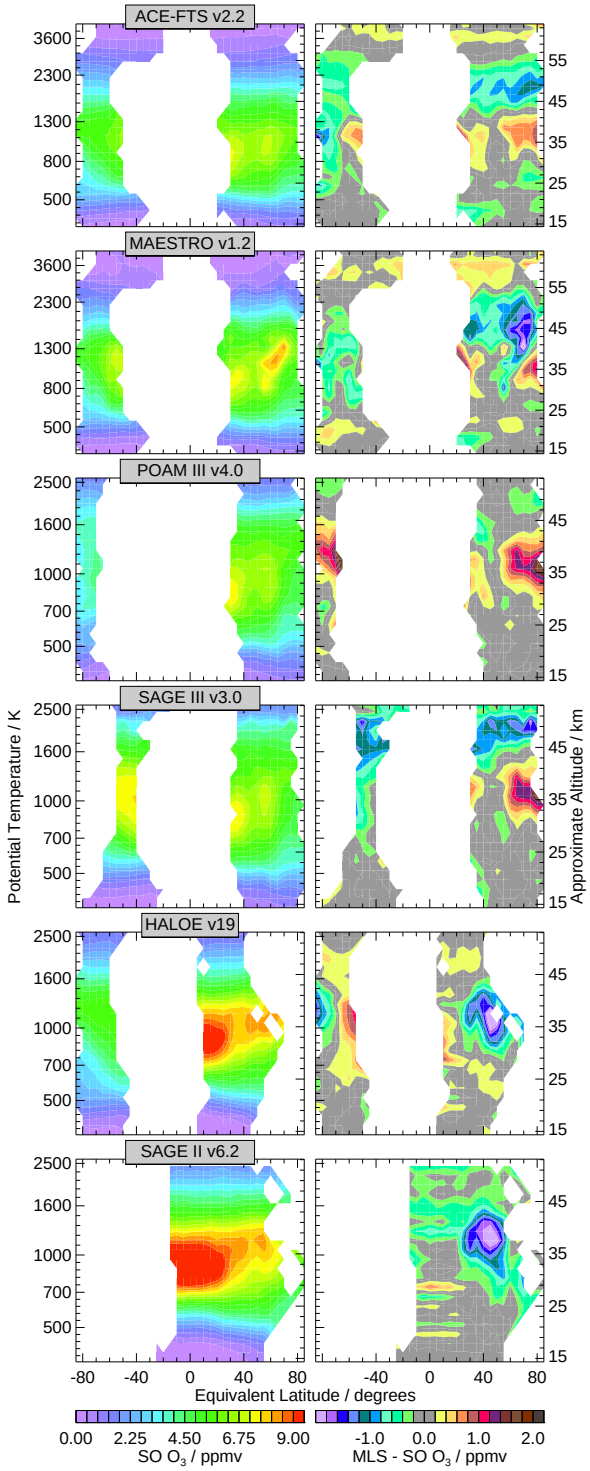

Figure 16. Global EqL/θ cross-sections for 10–16 March 2005 comparing MLS v2.2 O_3 with (top to bottom) ACE-FTS, MAESTRO, POAM III, SAGE III, HALOE, and SAGE II. Left panels show the solar occultation instruments' O_3 and right panels the MLS-solar occultation instrument O_3 difference (ppmv). For comparisons with ACE-FTS and MAESTRO, GEOS-5 DMPs are used for EqL/θ mapping; others comparisons use MetO DMPs. MLS/ACE comparisons are shown from 360 through 4430 K; others are 360 through 2500 K (the top limit of the the MetO DMPs).

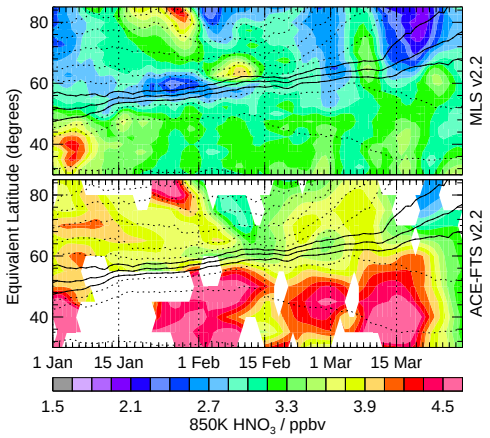

Figure 17. As in Figure 13, but for MLS v2.2 (top) and ACE-FTS (bottom) HNO_3 (ppbv) at 850 K, using GEOS-4 DMPs.

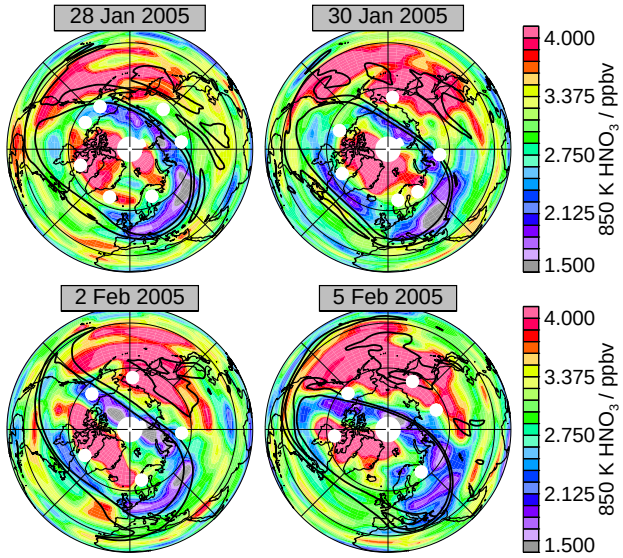

Figure 18. Maps of MLS v2.2 HNO_3 (ppbv) at 850 K for 28 and 30 January and 2 and 5 February 2005, with ACE-FTS observation locations (white dots) overlaid. PV contours in the vortex edge region are overlaid in black. Projection is orthographic, with 0° longitude at the bottom; latitude range is from 0 to 90°N. White space above ∼82°N is region not sampled by MLS.

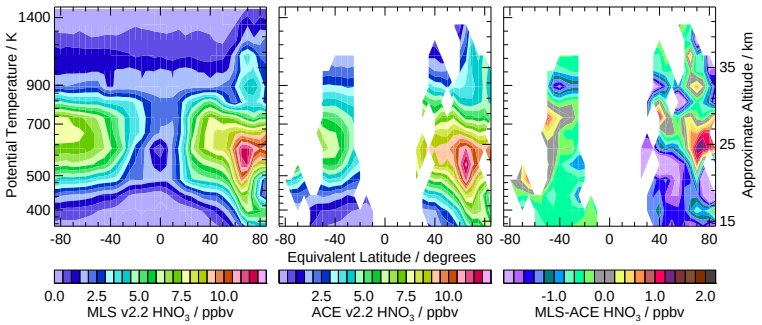

Figure 19. As in Figure 9, but for MLS v2.2 and ACE-FTS HNO_3 (ppbv) for 25–31 January 2005, using GEOS-5 DMPs. Vertical range is 400-1600 K.

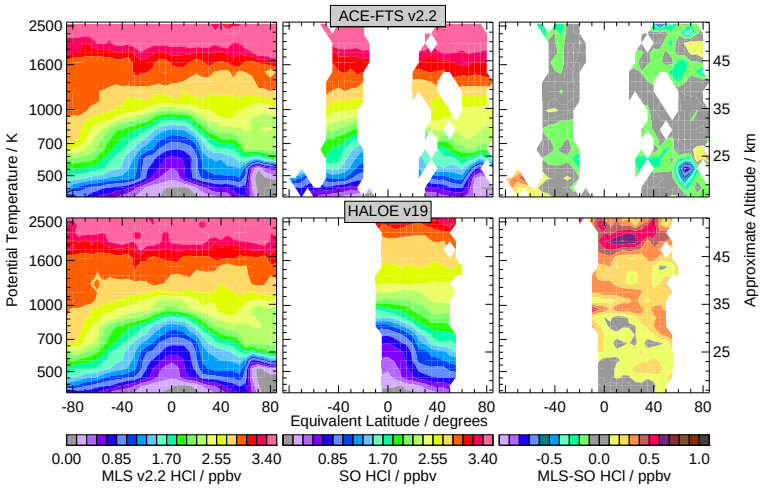

Figure 20. As in Figure 9, but for MLS v2.2, ACE-FTS, and HALOE HCl (ppbv) for 25–31 January 2005. ACE-FTS comparison uses GEOS-5 DMPs, HALOE comparison uses MetO DMPs. Vertical range is 400-2500 K.

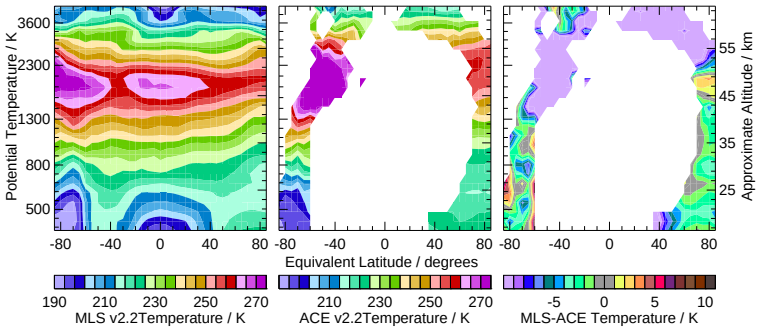

Figure 21. As in Figure 9, but for 17–24 September 2005 MLS v2.2 and ACE-FTS temperatures, using GEOS-5 DMPs. Vertical range is 360 to 4300 K.

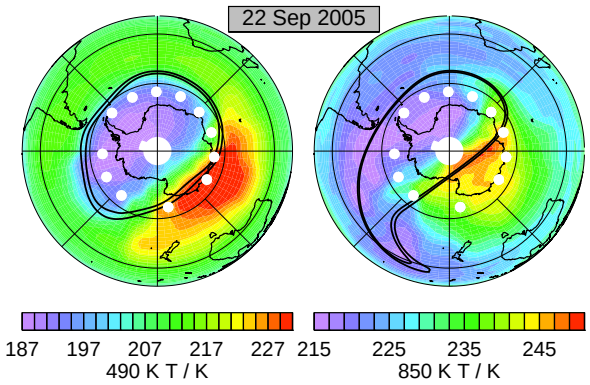

Figure 22. Maps of MLS v2.2 Temperature (colors, K) on 22 September 2005 at (left) 490 K and (right) 850 K. Overlaid contours are 1.4 and 1.8×10^{-4} s^{-1}sPV. White dots show ACE observation locations.